

Aerosol (-Radiation) Remote Sensing

Ritesh Gautam

rgautam.iitb@gmail.com

* Matlab scripts to analyze Level1b (radiance/reflectance) and Level-2 AOD data for the dust storm case study is shared at the below dropbox link. The link also contains the Level1b (MYD021km) and Level-2 (MYD04) files:

<https://www.dropbox.com/sh/mjsrz0ziolub9w2/AADgTC8IG6ei0GgW1dRsgq5pa?dl=0>

Outline

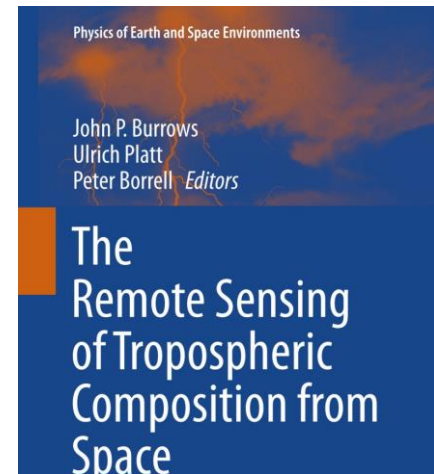
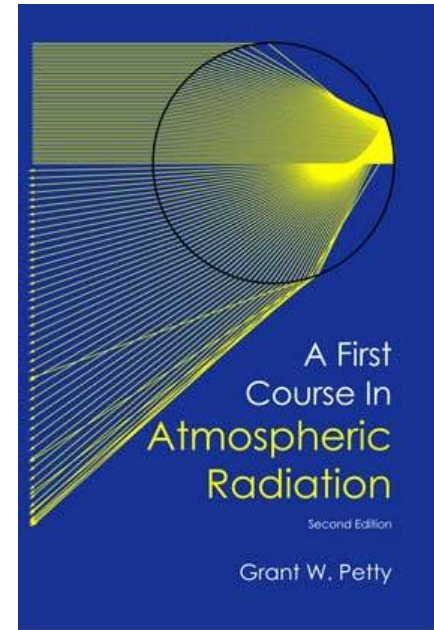
- (quick) Fundamentals of optical remote sensing
- Aerosol scattering principles
- Satellite remote sensing of aerosols over dark (ocean, vegetation) and bright surfaces (deserts, clouds, snow)

References

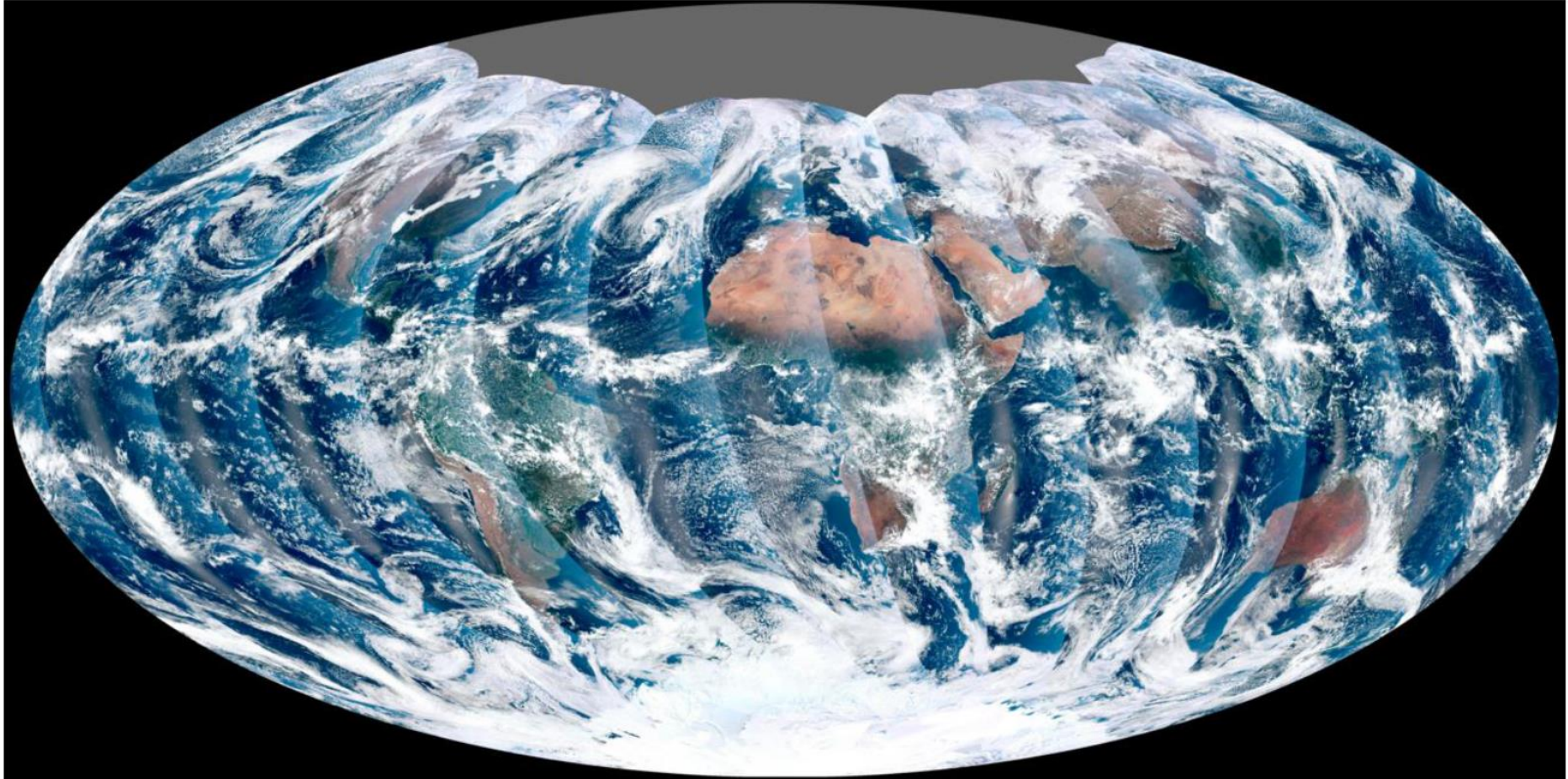
Chapters 1-3 of Petty are quite useful in fundamental atmospheric radiation;
First three chapters are freely available from the publisher:

<http://www.sundogpublishing.com/wp-content/uploads/2012/01/AtmosRadCh1-3.pdf>

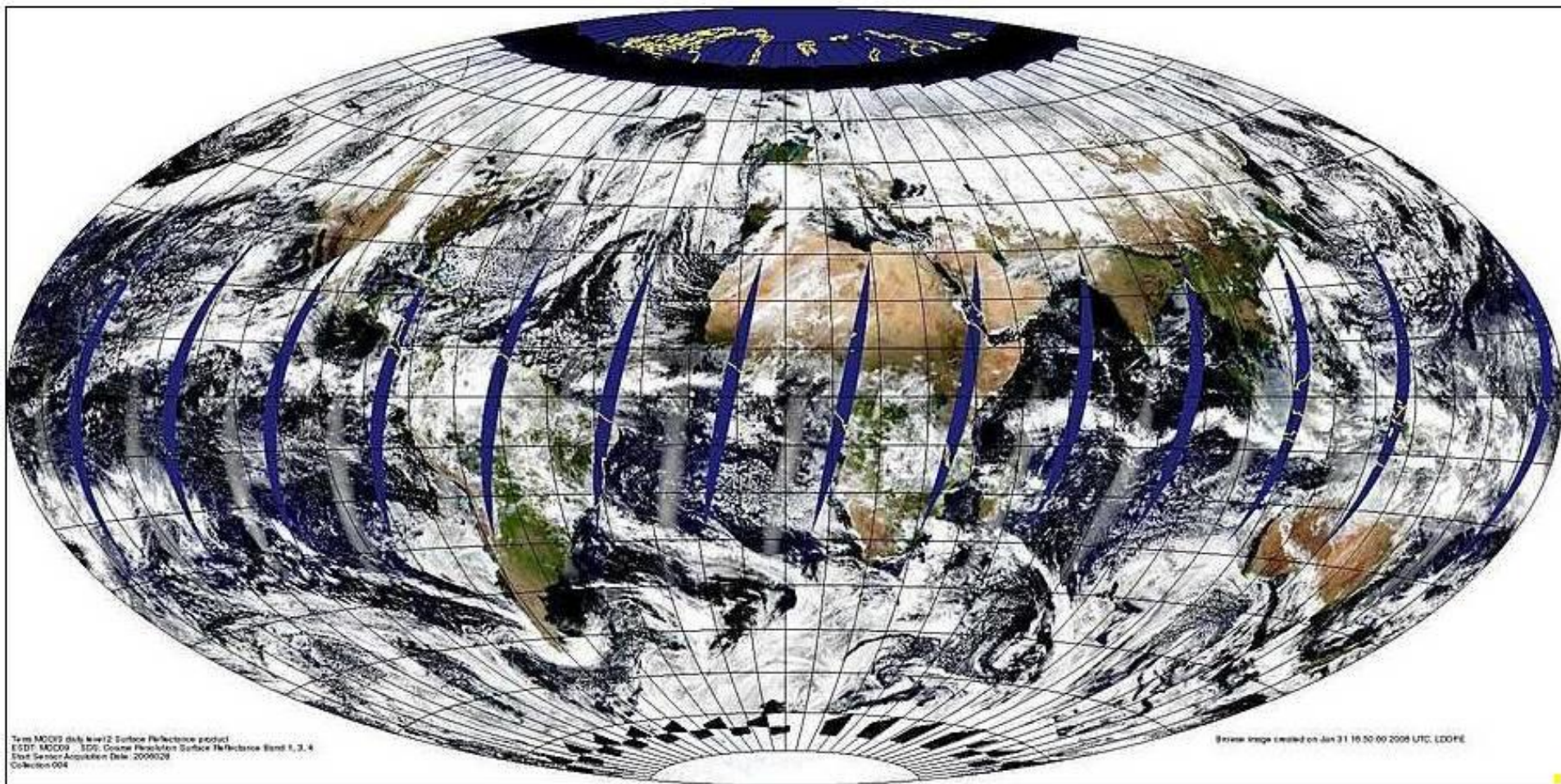
Chapters 5 and 6 from Burrows book are highly relevant for aerosol and cloud remote sensing.



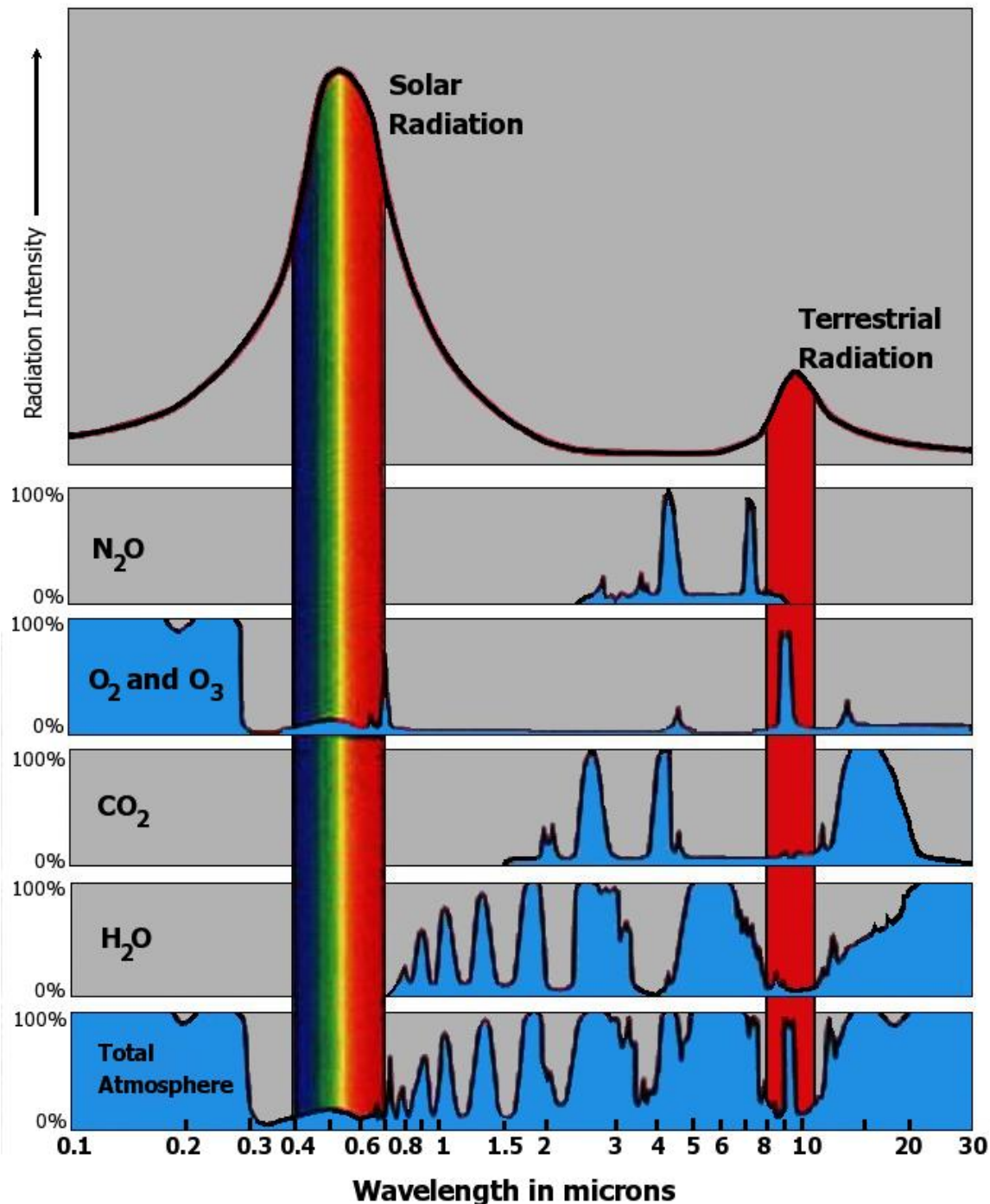
Global True-Color (RGB) Image by VIIRS instrument



- The above satellite image is taken by the VIIRS sensor onboard NPP satellite. This is the first image captured on 26 November 2011 by the VIIRS sensor, upon the launch of NPP satellite. Since this image corresponds to the winter-time, there is a large data gap over the North Pole (refer to previous slide as to why this occurs).
- Additionally, a key advantage of the NPP/VIIRS sensor is that its swath width is larger than MODIS, and as a result, there are no orbital gaps especially in the equatorial regions (as seen in the case of MODIS).
- Another interesting observation from this image is the brightening of the scene near the edge of swath (in each orbit). This is associated with the oblique/large scan angle of NPP/VIIRS resulting in enhanced Rayleigh scattering.



Terra satellite, MODIS instrument, coverage of all instrument swaths during a single day
This is a global mosaicked image of all granules acquired by MODIS in one day.
Note: this image is from January 31 when there is hardly any sunlight over the North Pole.
As a result, MODIS (a passive sensor) cannot make any measurements due to the absence of reflected solar radiation, and thus there is absence of data over the North Pole, in contrast to data recorded over south Pole. The opposite pattern will be true for summer season.



Visible part of Solar Radiation is largely unaffected atmospheric gases, but it is influenced by particle scattering (due to aerosols and clouds).

Longwave radiation is influenced by absorption due to gases present in the atmosphere such as CO₂, water vapour, methane, etc.

Backward Scattering View

This photo captured on the rooftop of CSRE building, IIT Bombay is taken around 3:30pm when the Sun is at the back side of the camera. In other words, we are looking in the direction opposite to the Sun (Sun is in the other part of Sky).

There are two interesting features:

1. The Sky above appears blue (less polluted), which is because of the backward scattering concept such that aerosols scatter much weakly in the backward scattering domain).
2. Vegetation (tree leaves etc.) appear brighter in this photo associated with the “hotspot” phenomenon of how vegetation scatter light.



Forward Scattering View

This photo was captured alongside the previous one, around 3:30pm, when the Sun is located in the front side of the camera. In other words, we are looking in the direction where the Sun is located just outside of this photo.

There are two interesting features:

1. The Sky above appears hazy/dirty white (more polluted), which is because of the forward scattering concept such that aerosols scatter much strongly in the forward scattering domain).
2. Vegetation (tree leaves etc.) appear darker in this photo as compared to backward scattering.



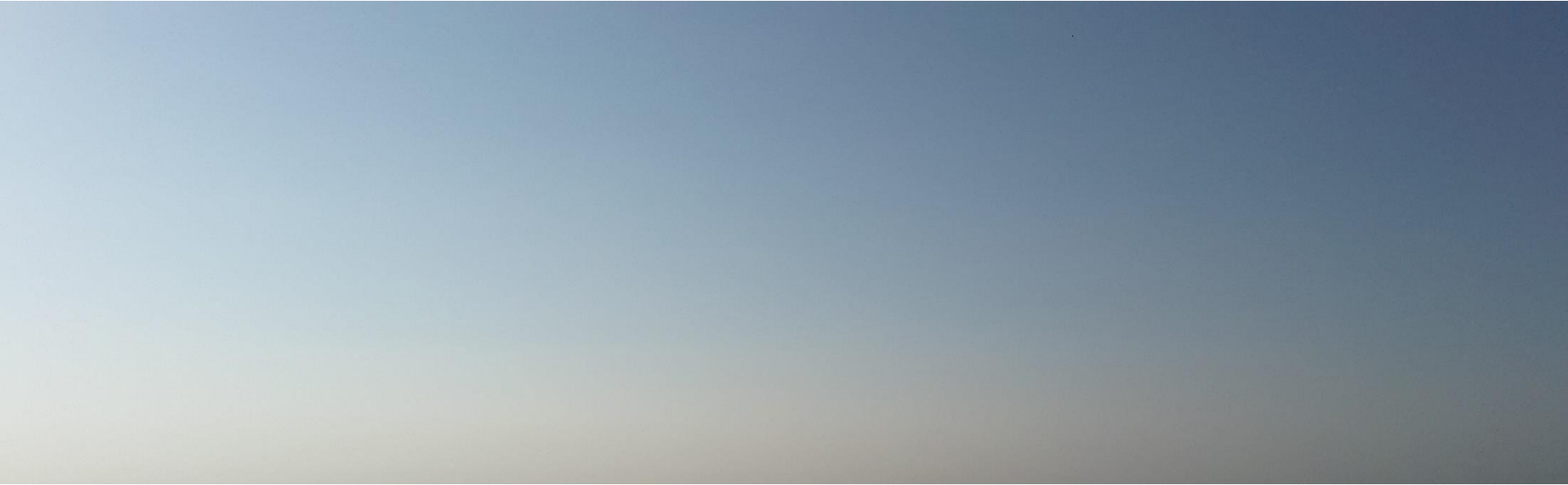
Backward Scattering View

(This is another example of backward scattering. Photo taken ~4pm atop Kanheri Caves, Mumbai)



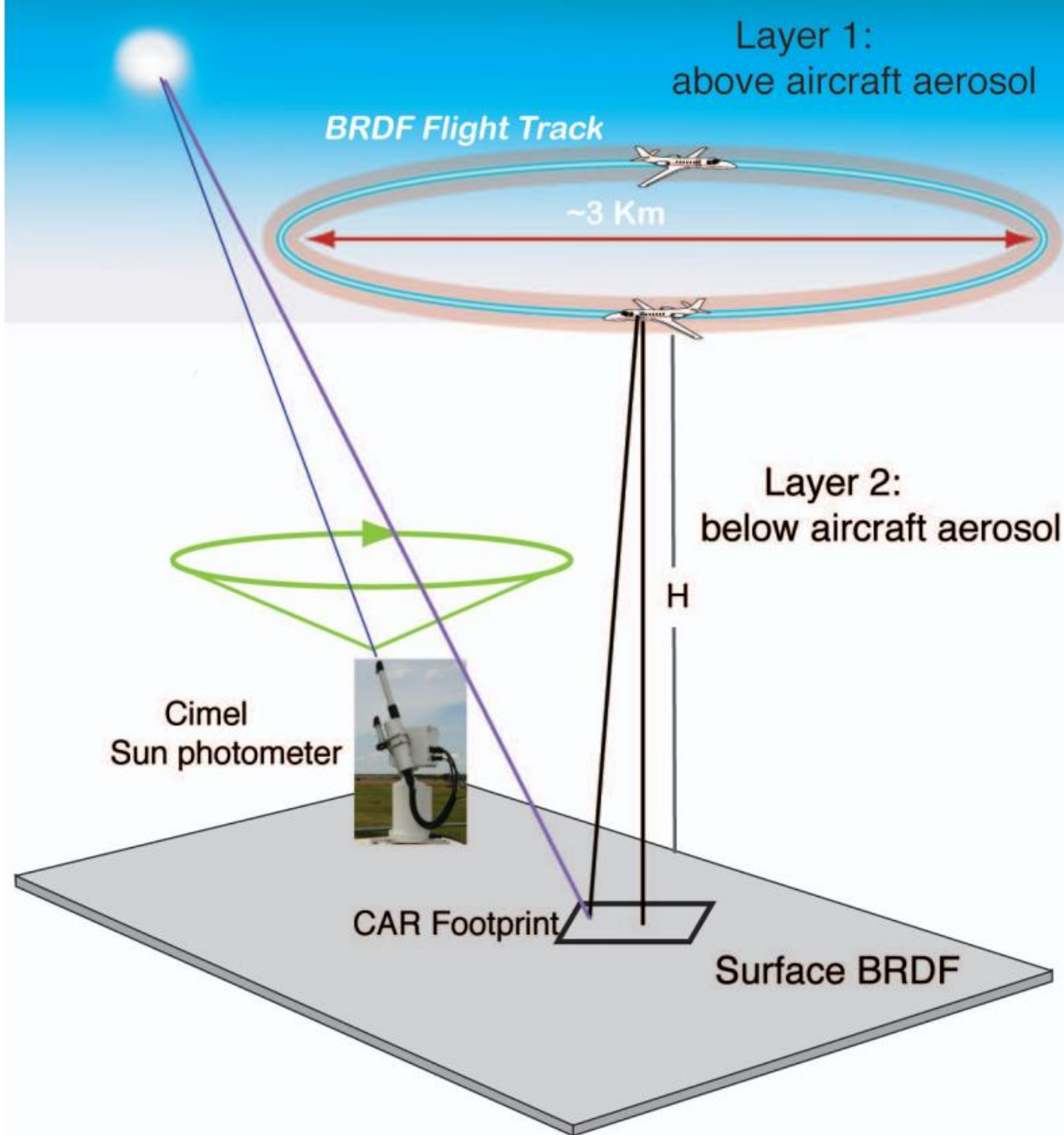
Forward Scattering View

(This is another example of forward scattering. Photo taken ~4pm atop Kanheri Caves, , Mumbai)



This is an example of airborne remote sensing where a remote sensing instrument is mounted aboard an aircraft flying at an altitude of 3km, above ground.

The aircraft is making circular transects allowing the sensor to make multi-angular measurements (from 0 to 360 degrees along the azimuthal plane).



The remote sensing instrument is installed in the “nose” of the aircraft. The sensor scans the sky and surface and takes measurements along the zenith plane from 0 to 180 degrees.

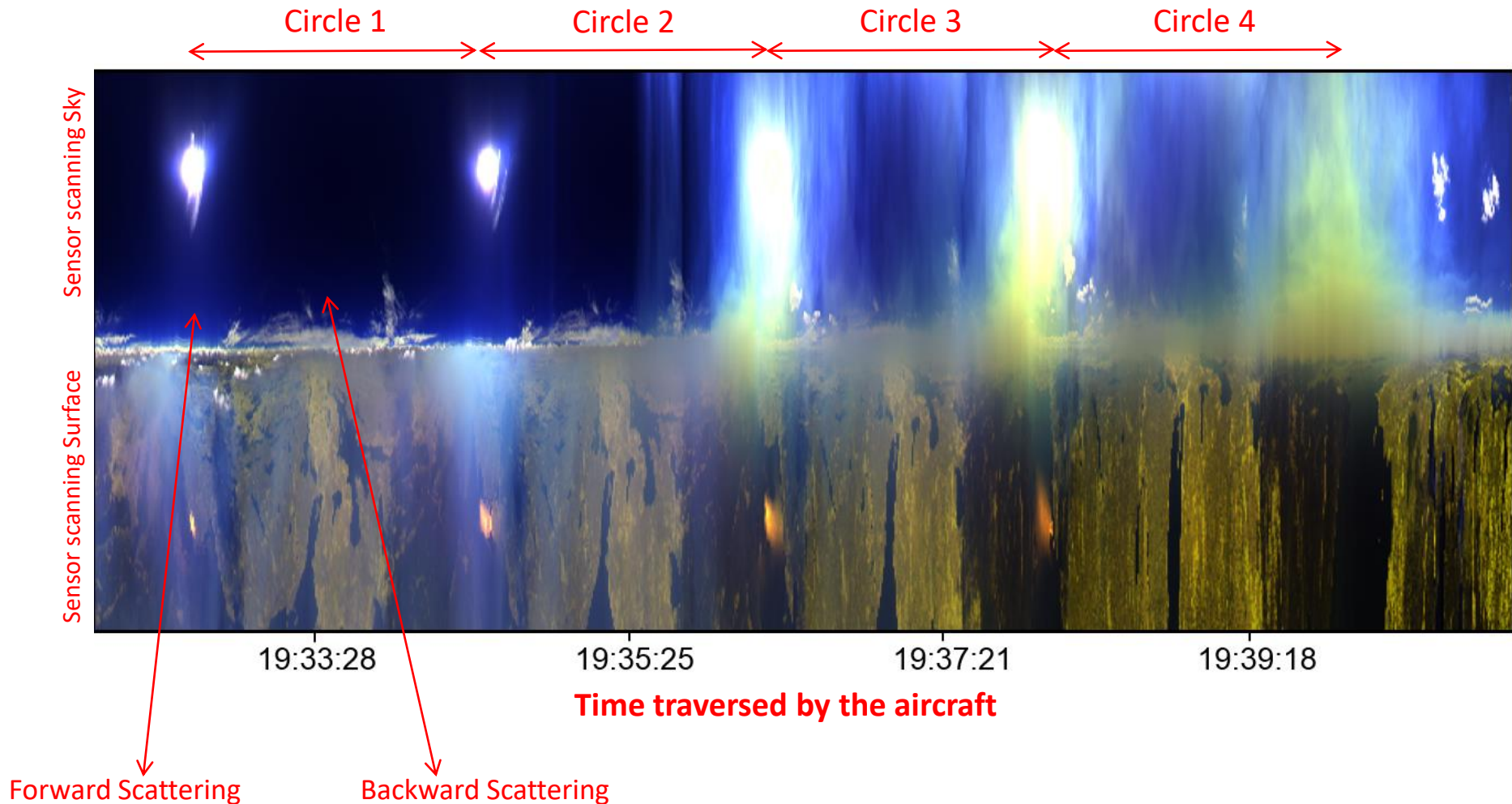
NASA P-3B Aircraft



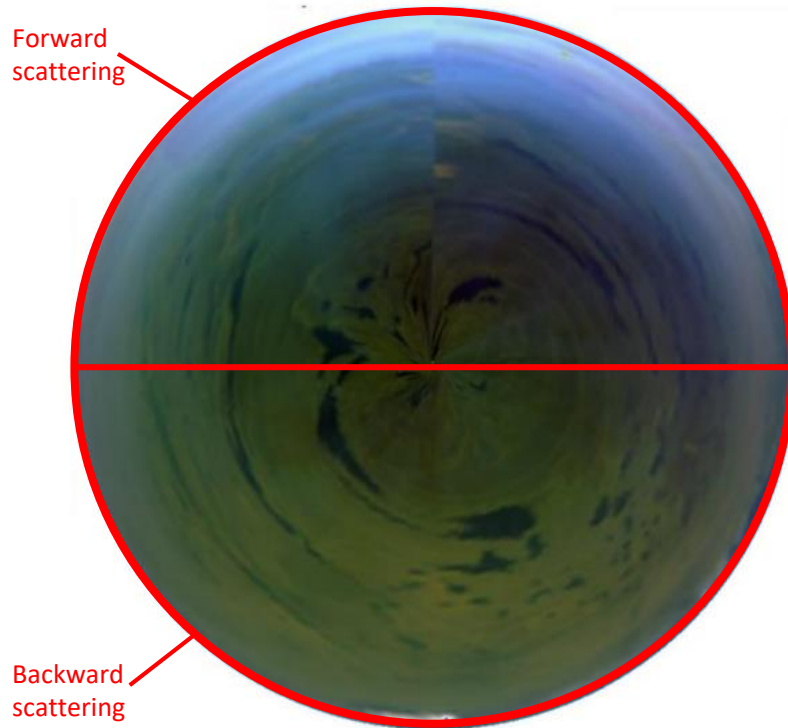
Remote Sensing Instrument

Below image is created using measurements from the airborne sensor (described in previous slides). The aircraft makes four circular transects, and therefore the sensor not only makes measurements in the 0-360 deg azimuthal plane, but also in the zenith plane (from sky to surface). Looking at the Sun corresponds to forward scattering.

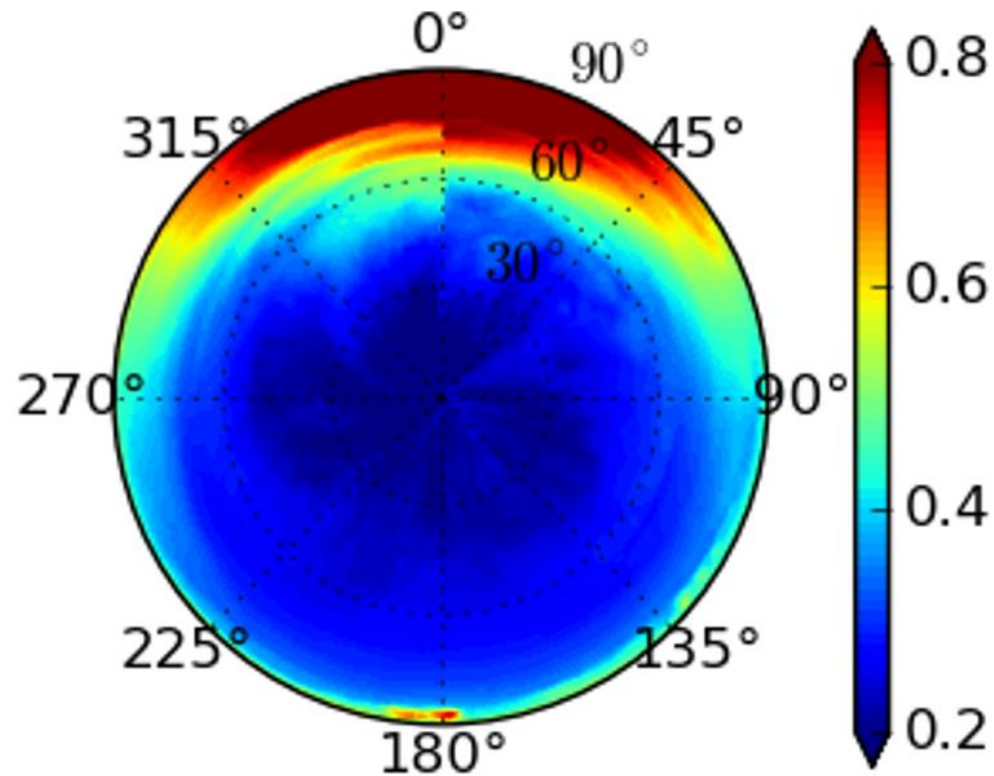
Note: the aircraft is descending down (spiralling down) and therefore the sensor encounters heavy aerosol loading, resulting in enhanced aerosol scattering (hazy conditions) in circle 3 and circle 4 (especially in forward scattering view).



False-color image shown in polar form (enhanced aerosol scattering is observed in forward scattering direction). This image is created from reflectance data obtained from circular aircraft measurements.

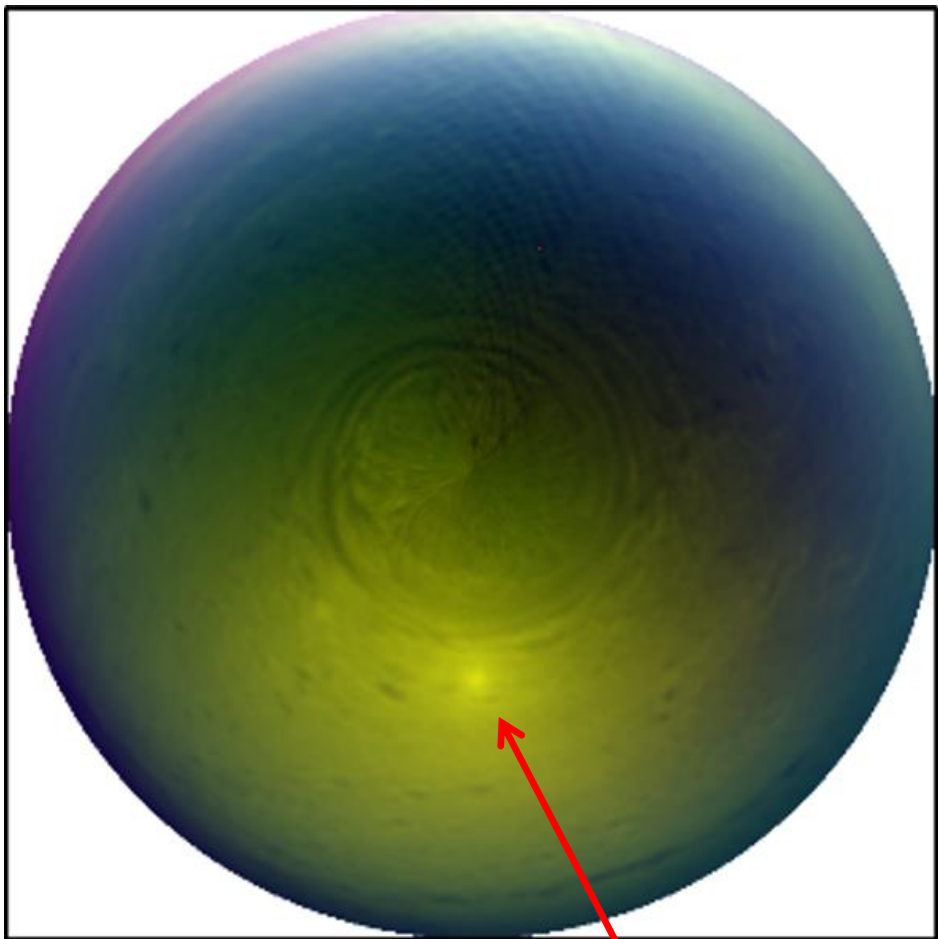


**Reflectance at 0.47 micron
(higher values of reflectance apparent in
forward scattering direction)**



- 0-360 deg corresponds to circular measurements (azimuthal plane)
- 0-90 deg corresponds to measurements over surface, where 0° indicates when sensor is directly looking down, while 90° indicates when sensor is viewing the horizon (just above the surface)

Another example showing the occurrence of hotspot associated with enhanced reflectance of vegetation observed in backward scattering domain.



“Hotspot”

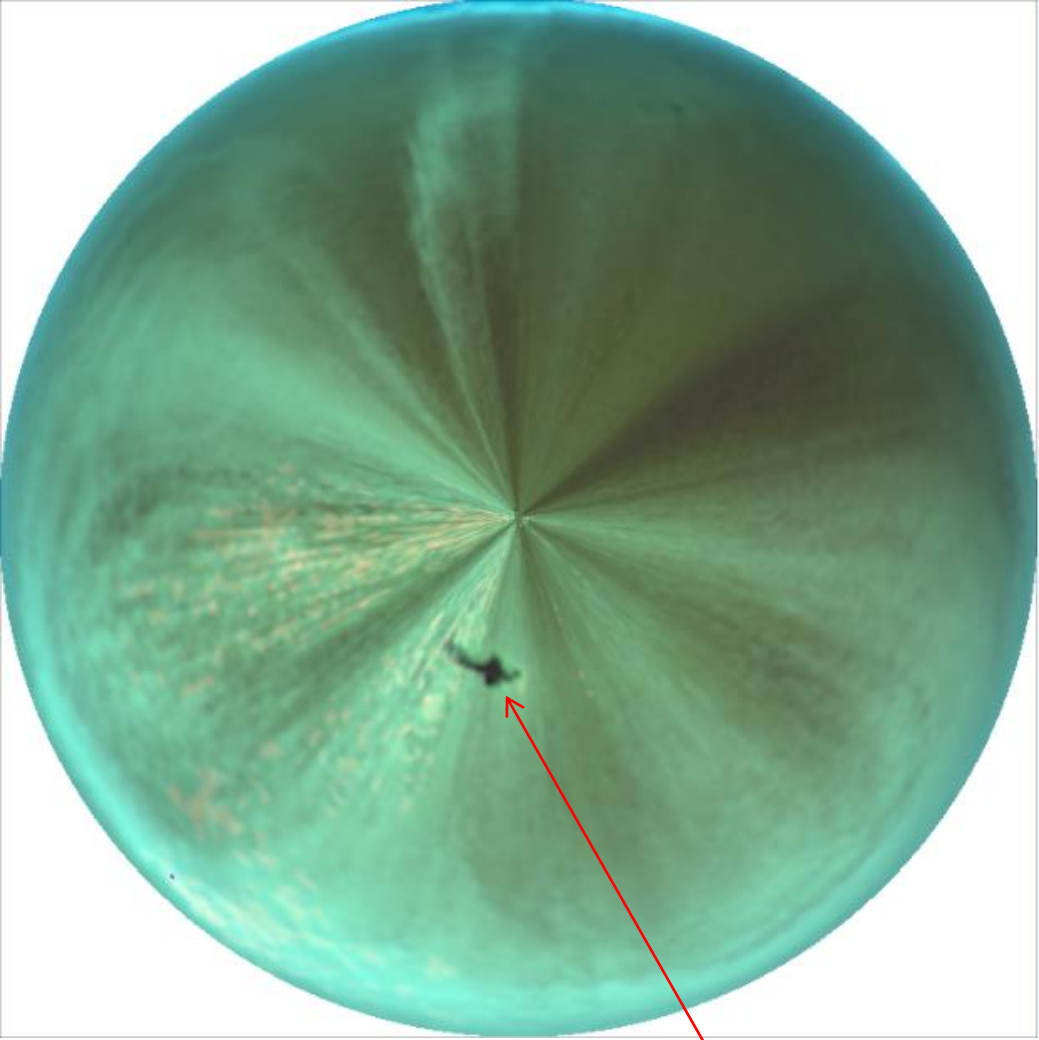
Forward Scattering domain



Backward Scattering domain



A rather compelling case of forward and backward scattering, as evidenced by the formation of shadow of aircraft in the backward scattering domain.



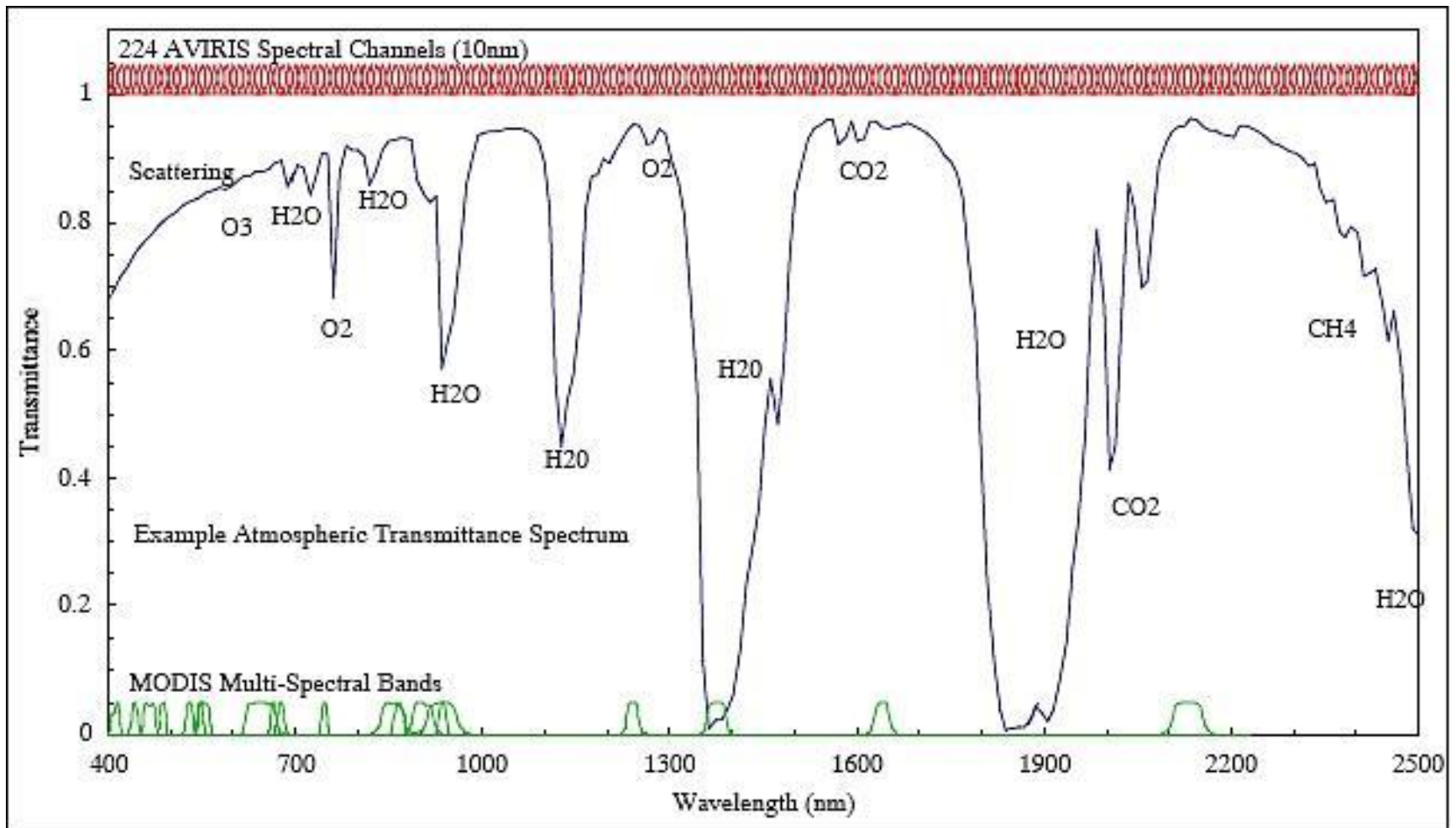
Shadow of the aircraft

Impact of Atmospheric Gases Absorption on Transmittance Spectrum

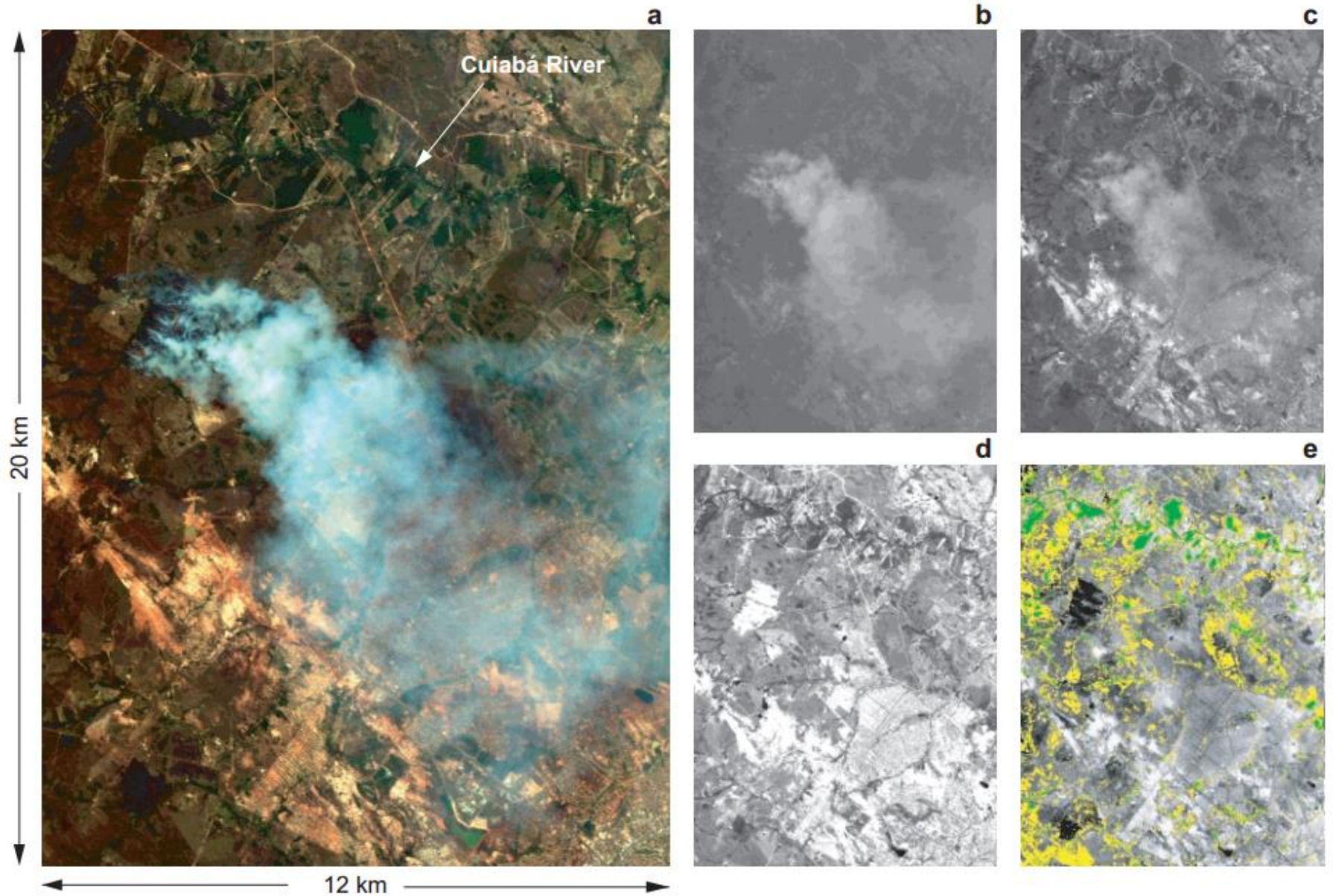
For example, Oxygen is strongly absorbing at 760nm, while water vapour is absorbing at multiple wavelength bands in nearIR (940nm, 1380nm, etc.)

Transmission = 1 (100%), indicates atmosphere is totally transparent (no extinction of light either from absorption or scattering)

Transmission = 0, indicates atmosphere is totally opaque.



Aerosol scattering/absorption affecting at-sensor Radiance



Aerosol scattering/absorption affecting at-sensor Radiance

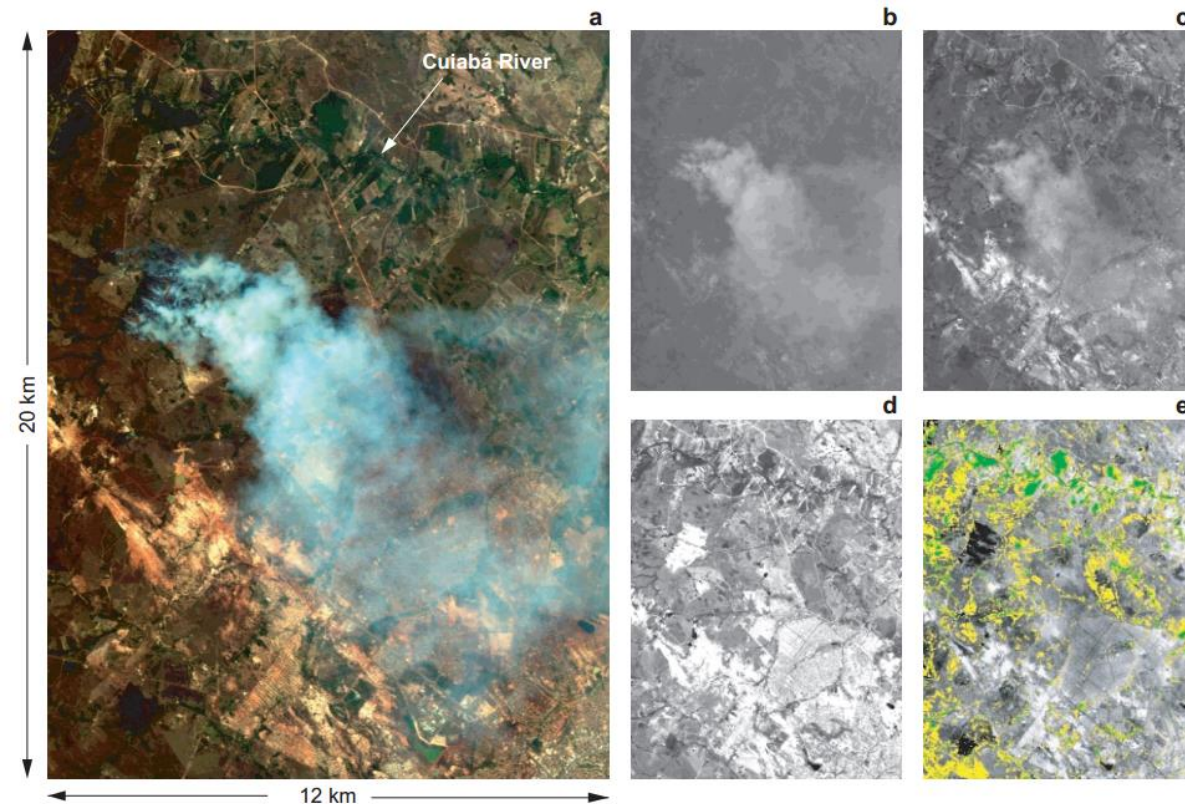


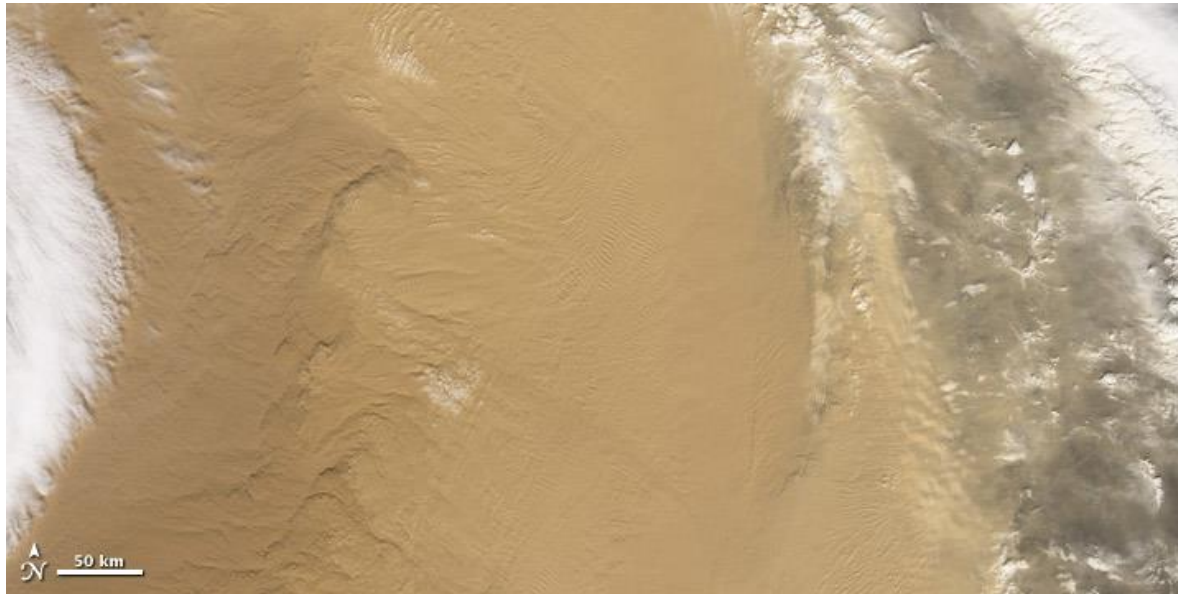
FIG. 4. AVIRIS images acquired near Cuiabá, Brazil, on 25 Aug 1995. (a) A red–green–blue composite of 0.66, 0.55, and 0.46 μm bands; (b)–(d) images for individual bands. Panel (b) applies to 0.46 μm , which is especially sensitive to smoke, (c) to 0.66 μm , also sensitive to smoke but with brighter surface reflectance, and (d) to 2.13 μm , which shows both hot ground and bright land. (e) Location of all dense dark vegetation within this scene, defined as pixels for which the surface reflectance $A_g(2.13 \mu\text{m}) \leq 0.10$ (green pixels) or $0.10 < A_g(2.13 \mu\text{m}) \leq 0.15$ (yellow pixels). The background image on which the dark vegetation pixels are overlaid is the AVIRIS image at 0.86 μm , for which vegetation is bright and burn scars dark.

A sequence of figures (a-e) shows the different images as a function of wavelength. Note, how the reflectance changes as one approaches the absorption bands and the surface disappears.

The reflection from the vegetated surface increases after 0.66 micron and surface features become evident (recall vegetation is more reflective in near-IR and shortwave-IR, e.g. 2.13micron- figure d). At the same time, smoke particles are small in size and interact efficiently with the light at shorter wavelengths (<0.66micron), causing enhanced scattering.

Above 0.66 micron the low level smoke becomes less opaque and more transparent, and we are able to see the underlying more clearly at longer wavelengths. The fire on the ground becomes evident at the longer wavelengths as thermal emission supplements solar reflection.

Mineral Dust (appears as yellow-brown associated with enhanced absorption at blue wavelengths)



Biomass burning Smoke (appears as gray)

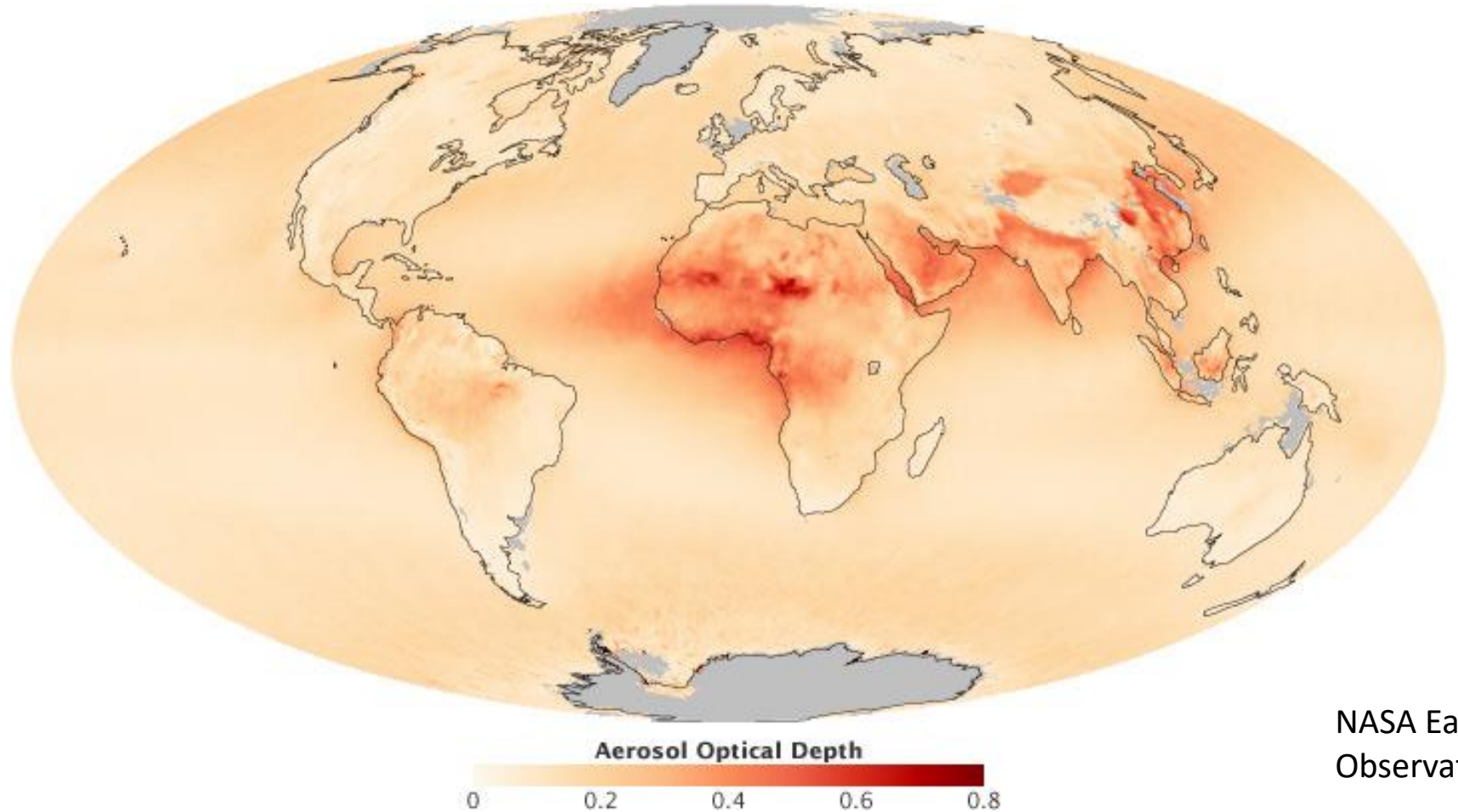


Various types of Aerosols

- Sea Salt (Ocean/Sea Spray) -- **NATURAL**
- Mineral Dust (soil, desert dust) -- **NATURAL**
- Sulfate (industrial/urban emissions) -- **ANTHROPOGENIC**
- Carbonaceous (soot/black carbon, source: industrial/urban/biomass burning emissions) -- **ANTHROPOGENIC**
- Volcanic Ash -- **NATURAL**



Example of Aerosol Optical Depth retrieved by MISR (multi-angular measurements)



The typical range of AOD is from 0 to 2, with higher values indicating larger aerosol concentration in atmosphere. Missing values (shown in gray) indicate where AOD is not retrieved over snow-covered regions including polar regions, Greenland, parts of Himalaya, Tibetan Plateau.

Note: aerosols can only be retrieved from satellites when there are no clouds present in the same pixel. For persistently cloudy regions, e.g. areas around Indonesia, there are hardly any aerosols retrieved by satellites because of the frequent cloud-cover. This does not mean there are no aerosols present in the atmosphere, but only suggests that aerosol observations from space can be only made in cloud-free conditions.

Aerosol Optical/Radiative Properties

- Aerosol Optical Depth
- Angstrom Exponent
- Single Scattering Albedo
- Phase Function

Interaction of Radiation and Aerosol

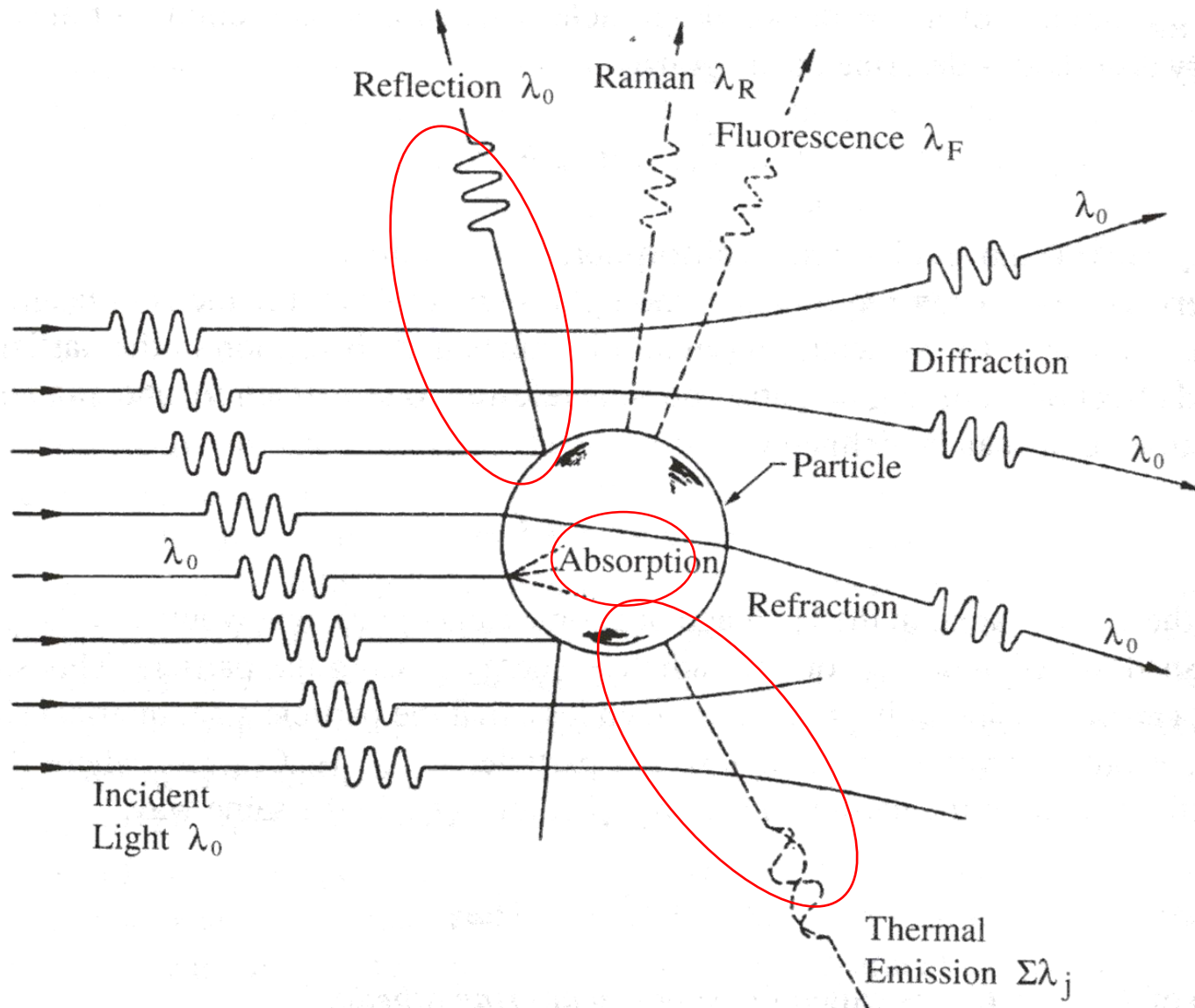


FIGURE 22.1 Mechanisms of interaction between incident radiation and a particle

The extinction coefficient (b_{ext}) represents the sum of the extinctions from gases and particles, each of which can in turn be divided into extinction due to absorption or scattering.

$$b_{\text{ext}} = b_{\text{gas}} + b_{\text{particles}} \quad (\text{extinction due to gases and particles})$$

$$b_{\text{ext}} = b_{\text{abs}} + b_{\text{scatt}} \quad (\text{extinction refers to attenuation of light due to absorption and scattering})$$

$$b_{\text{abs}} \text{ (gases)} = \text{Beer's Law absorption}$$

$$b_{\text{scatt}} \text{ (gases)} = \text{Rayleigh Scattering}$$

$$b_{\text{abs}} \text{ (particles)} = \text{Usually} < 10\% \text{ of extinction}$$

$$b_{\text{scatt}} \text{ (particles)} = \text{Mie Scattering} = (b_{\text{sp}})$$

Aerosol optical depth (AOD), τ is a measure of the extinction caused by scattering and absorption, where 'z' is the altitude (typically z ranges from surface to top of atmosphere):

$$\tau = \int b_{\text{ext}}(z) dz \quad (\text{unitless})$$

AOD is unitless. The integral is from surface to top of atmosphere.

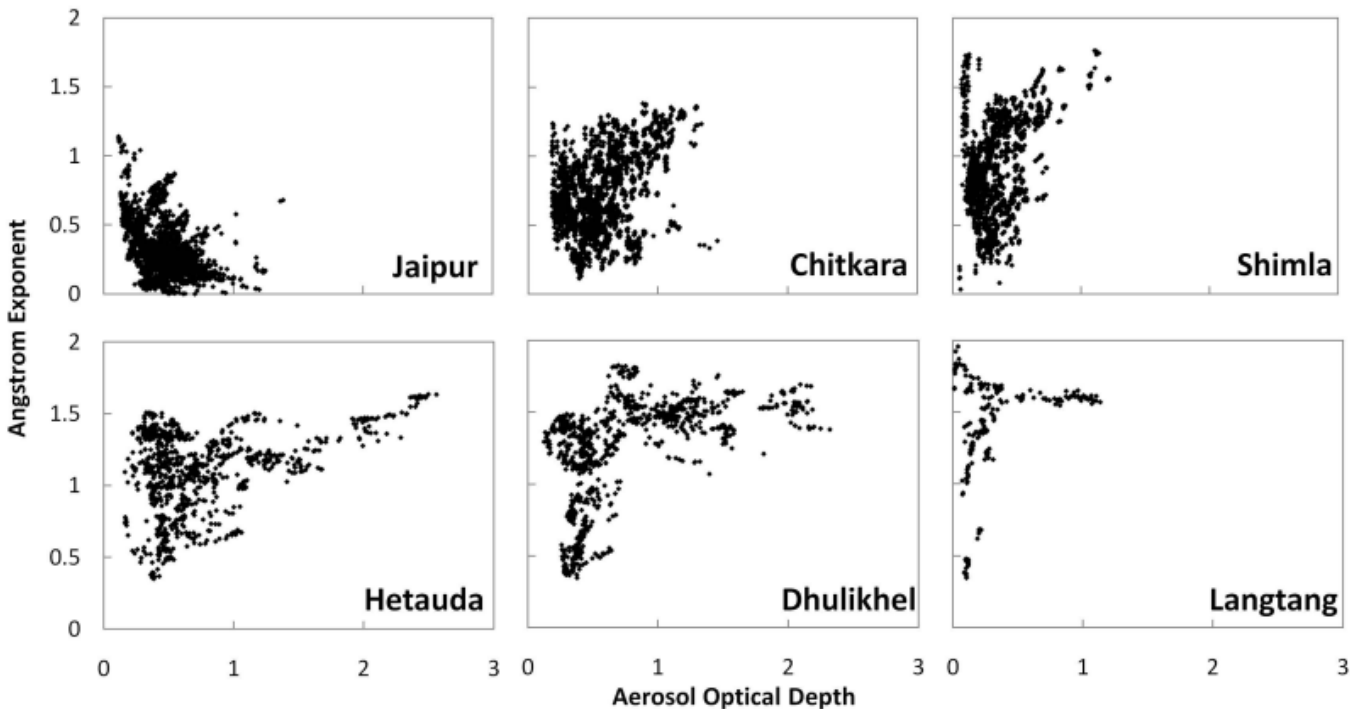
Angstrom exponent, α , is a measure of the size distribution, describes the dependency of the aerosol optical thickness on wavelength. For urban aerosols (fine particles) $\alpha > 1.0$, for dust storms (coarse particles) $\alpha \ll 1.0$. (λ_0 is shorter wavelength while λ is longer wavelength)

$$\frac{\tau_\lambda}{\tau_{\lambda_0}} = \left(\frac{\lambda}{\lambda_0} \right)^{-\alpha} \quad \alpha = - \frac{\ln \frac{\tau_\lambda}{\tau_{\lambda_0}}}{\ln \frac{\lambda}{\lambda_0}}$$

From the scatter plots, shown on left, between Aerosol Optical Depth, or AOD (x-axis) and Angstrom Exponent (y-axis):

For Jaipur, majority of the AOD data is associated with Angstrom Exponent less than 1, while most of the AOD data over Dhulikhel (near Kathmandu) is associated with values greater than 1.

Jaipur is close to the Thar desert in Rajasthan, and therefore is subjected to frequent dust storms, while Dhulikhel (Kathmandu) is far from the desert and is mostly affected by urban (fine) aerosols.

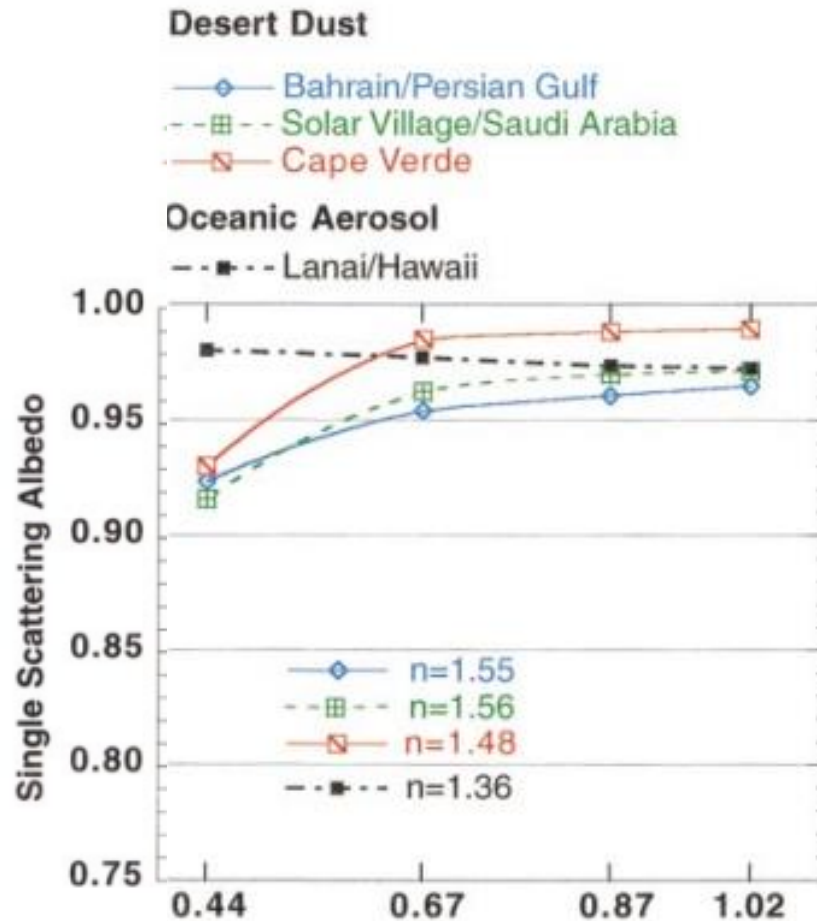


Single scattering albedo, w , is a measure of the fraction of aerosol extinction caused by scattering:

$$\omega = \frac{b_{\text{scatt}}}{(b_{\text{scatt}} + b_{\text{abs}})}$$

b_{scatt} is scattering coefficient and b_{abs} is absorption coefficient

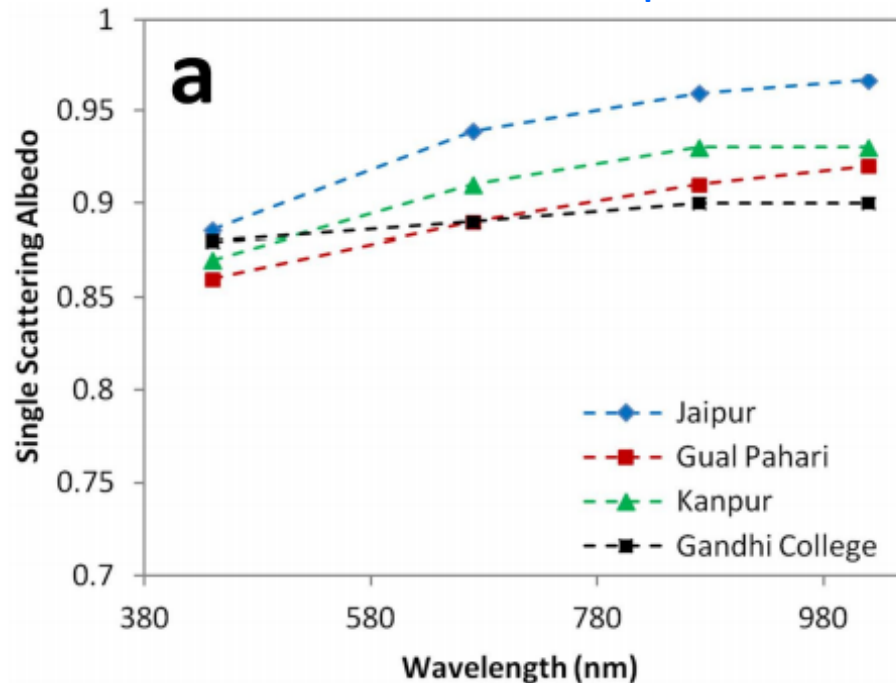
Single Scattering Albedo (SSA) value of aerosols ranges from 0 to 1. SSA=1 means 100% scattering aerosol (with no absorption).



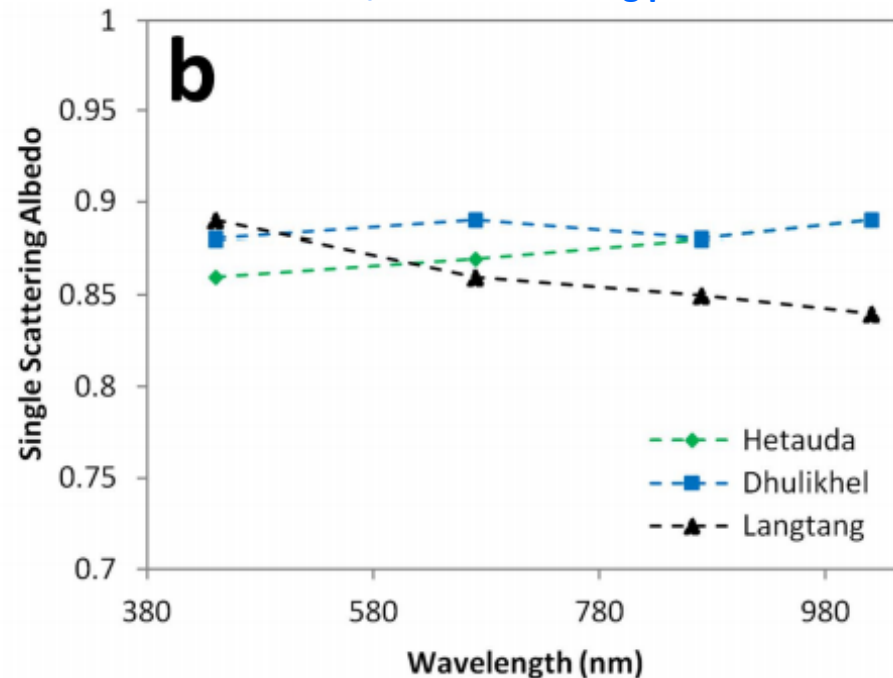
Single Scattering Albedo (SSA) over northern India and Nepal (April-May)

Dust aerosols contain haematite/iron oxide, which has strong absorption bands in the UV-blue spectrum. As a result, there is enhanced absorption at shorter visible (blue) wavelengths and thus decrease in SSA for dust-dominated atmosphere.

Dust dominated atmosphere



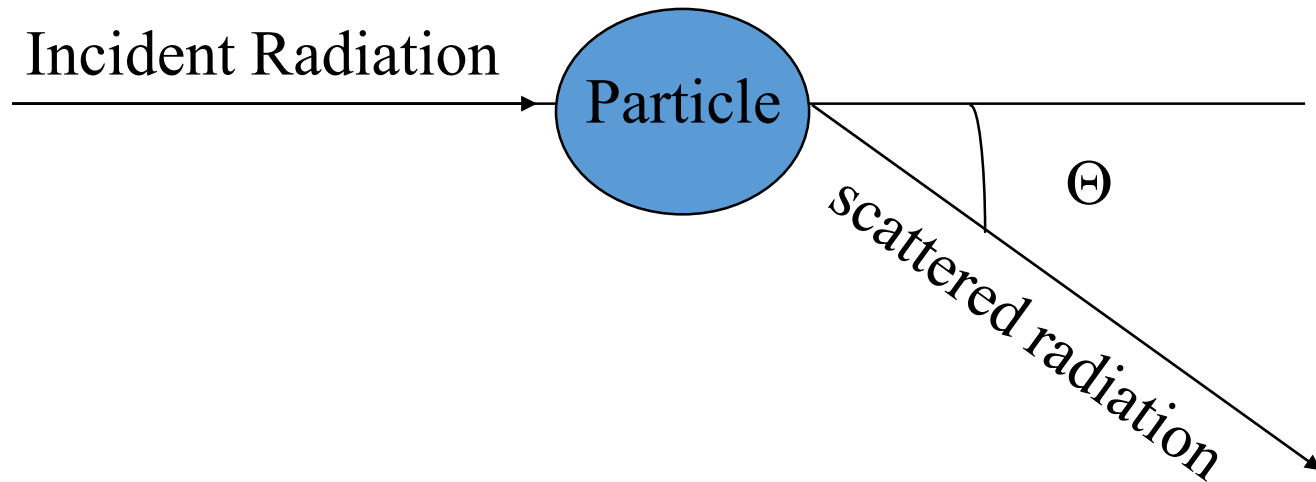
Urban/biomass burning pollution



SSA from AERONET sunphotometers at (a) Jaipur, Gual Pahari, Kanpur and Gandhi College in Northern India, and (b) at Hetauda, Dhulikhel and Langtang of Himalayan foothill/slope regions Nepal. The SSA from AERONET is retrieved at four wavelengths – 440 nm, 670 nm, 870 nm and 1020 nm. Values shown are mean SSA for the 2009 pre-monsoon measurement period.

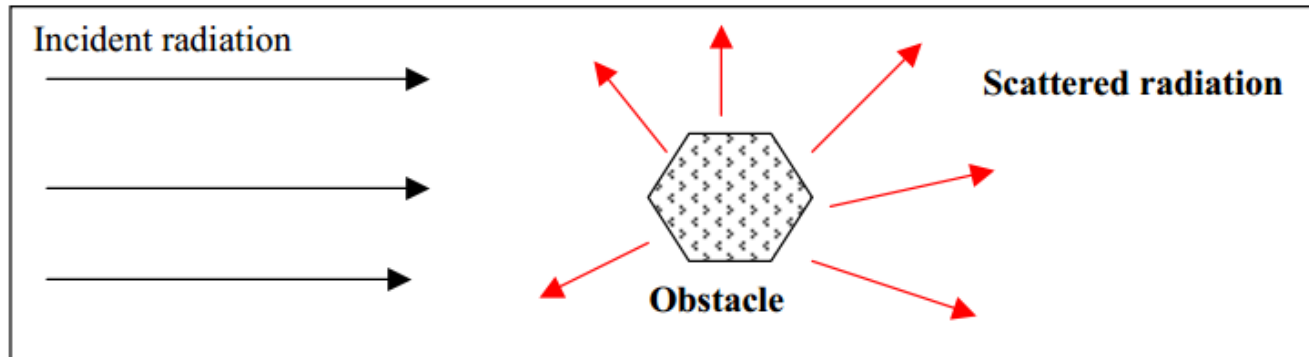
Scattering angle

The scattering angle, Θ , is the relative angle between the incident and the scattered radiation



NOTE: $\Theta = 0^\circ$ is often called forward scattering and $\Theta = 180^\circ$ is called backscattering.

Scattering by Particles



Scattering phase function $P(\cos\Theta)$ is defined as a non-dimensional parameter to describe the angular distribution of the scattered radiation as

$$\frac{1}{4\pi} \int_{\Omega} P(\cos \Theta) d\Omega = 1$$

where Θ is called the **scattering angle** between the direction of incidence and observation.

Phase function

The phase function, $P(\Theta)$, describes the distribution of scattered radiation for one or a set of particles. It is normalized such as:

$$\int_0^{2\pi} \int_0^{\pi} P(\Theta) d\omega = 4\pi$$

since
$$\int_0^{2\pi} \int_0^{\pi} P(\Theta) \sin(\theta) d\theta d\phi = 2\pi \int_0^{\pi} P(\theta) \sin(\theta) d\theta$$

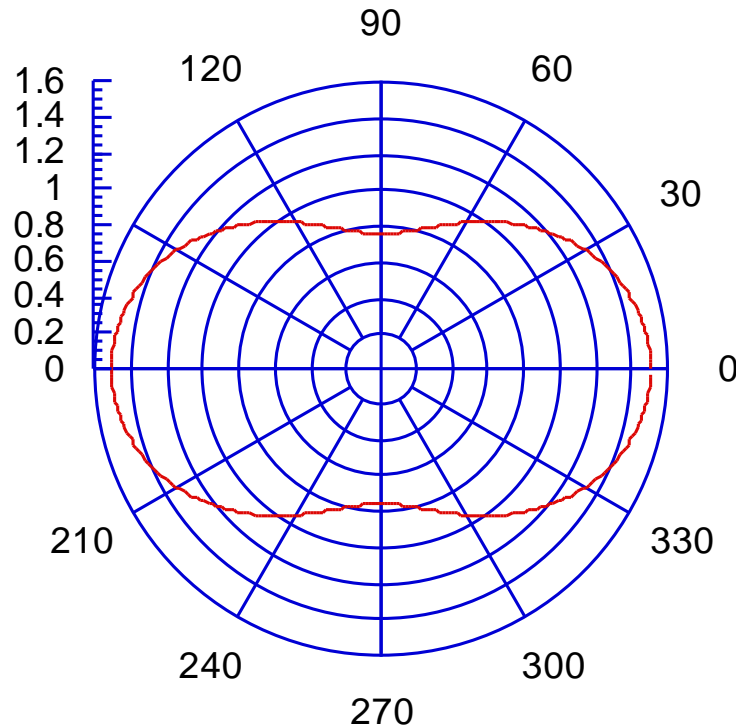
we have
$$\int_0^{\pi} P(\theta) \sin(\theta) d\theta = 2$$

Rayleigh/molecular scattering

Rayleigh or molecular scattering refers to scattering by atmospheric gases, in that case:

$$P(\Theta) = \frac{3}{4} (1 + \cos^2(\Theta))$$

Rayleigh Phase
Function




Rayleigh scattering is totally symmetric, i.e. amount of forward scattering and backward scattering is equal.

Rayleigh/molecular scattering

The Rayleigh reflectance, ρ_R , could be crudely approximated by:

Rayleigh Optical Depth


$$\rho_R^\lambda(\theta_s, \theta_v, \phi) \sim \frac{\tau_R^\lambda P(\Theta)}{4 \cos(\theta_s) \cos(\theta_v)}$$

Rayleigh molecules are 100% scattering. Therefore, the Rayleigh Single Scattering Albedo is always 1. This is different from the Aerosol Single Scattering Albedo (SSA), which varies between 0 and 1. Typically, the range of aerosol SSA is from 0.7 to 1.

The Single Scattering Albedo (SSA) is fundamentally dependent on the imaginary part of the complex index of refraction. SSA consists of two terms (scattering coefficient and absorption coefficient). The absorption coefficient is directly proportional to the imaginary part of refractive index.

Optical Properties of Small Particles

$$m = a + iN_i$$

m = complex index of refraction

' a ' indicates real part

' N_i ' indicates absorption (imaginary part)

The real part of the index of refraction is only a weak function of wavelength, while the imaginary part, N_i , depends strongly on wavelength.

Refractive indices of aerosol particles at $\lambda = 589$ nm

N_i indicates absorption (imaginary part)

Sea Salt
Aerosols

Sulfate
Aerosols

$m = a + iN_i$		
Substance	a	N_i
NaCl	1.544	0
H ₂ SO ₄	1.426	0
NH ₄ HSO ₄	1.473	0
(NH ₄) ₂ SO ₄	1.521	0
Black Carbon (soot)	1.96	0.66
Mineral dust	~1.53	~0.006

Sea Salt and Sulfate Aerosols are 100% scattering ($N_i=0$)

Mineral dust aerosols are moderately absorbing

Black carbon (soot) aerosols are strongly absorbing

Aerosol Impact on At-sensor Reflectance (Top-of-Atmosphere)

At-sensor reflectance, Apparent Reflectance and Top-of-Atmosphere (TOA) Reflectance imply the same quantity

California fire plumes



Pollution off U.S. east coast



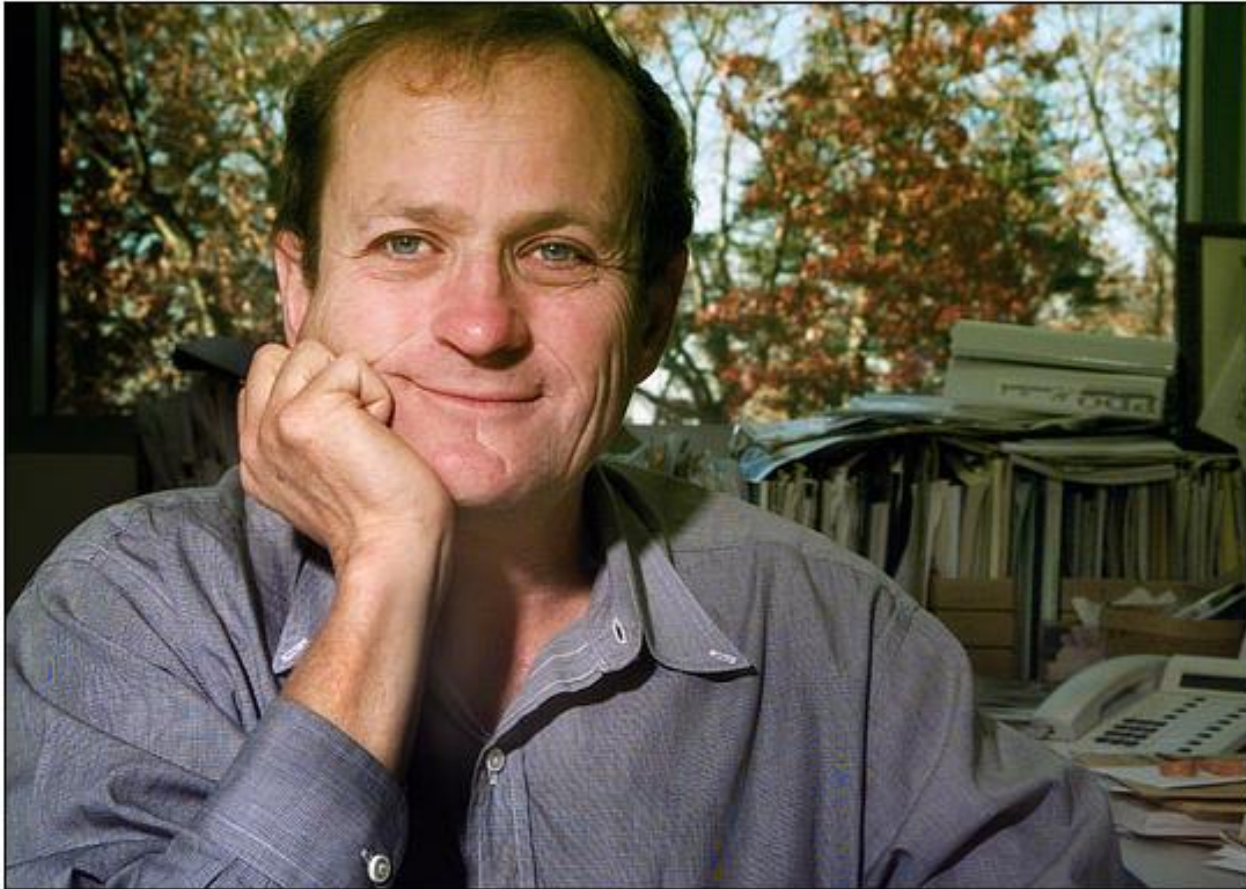
Dust off West Africa



Over which surface (ocean, vegetation, desert) are aerosols most easily detectable??

Yoram Kaufman

Pioneer in Aerosol Remote Sensing



Yoram Kaufman 1948-2006



Terra Launch (December 18, 1999)

Transfer of Radiation through the atmosphere

(Successive Orders of Scattering method, Vermote et al. 2002, 6S radiative transfer code)

**Atmospheric reflectance
(or path reflectance/radiance)**

Ground reflectance

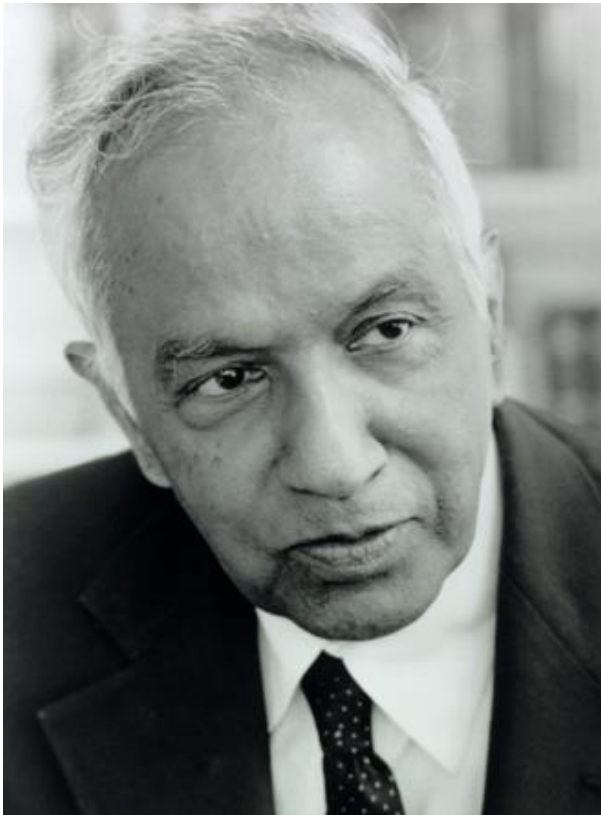
$$\rho(\theta_s, \theta_v, \phi) = \rho_{atm}(\theta_s, \theta_v, \phi) + T_{atm}(\theta_s) \cdot T_{atm}(\theta_v) \frac{\rho_{ground}}{1 - \rho_{ground} S_{atm}}$$

**Atmospheric
Transmissions**

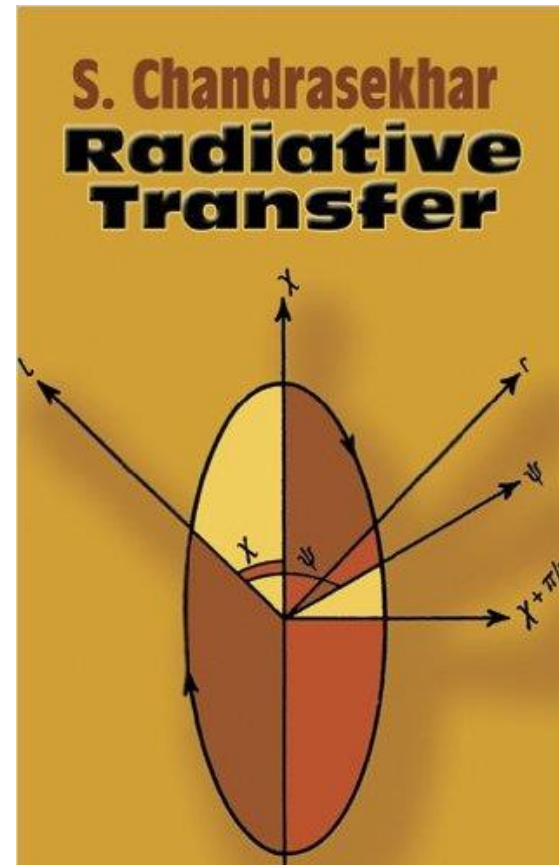
Reflectance at Top of Atmosphere (TOA)

Atmosphere albedo

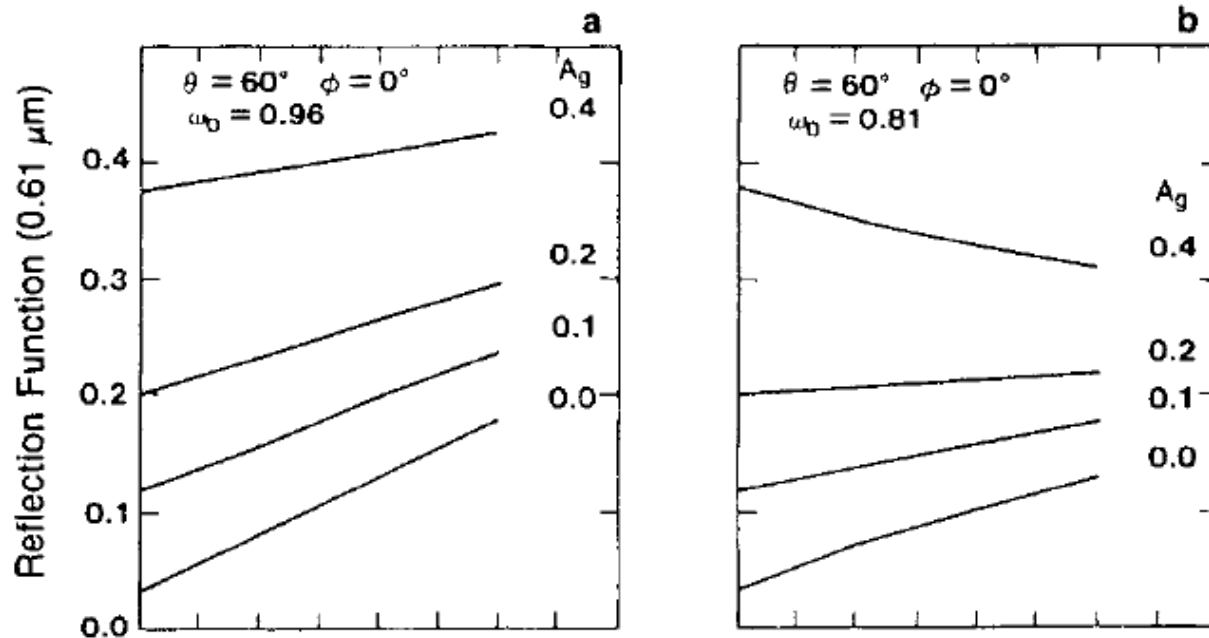
Subrahmanyan Chandrasekhar
(Nobel Laureate in Physics, 1983
Pioneer in several areas of Astrophysics,
including Radiative Transfer)



S. Chandrasekhar's seminal book on Radiative Transfer cited in over 10,000 publications



Changes in TOA Reflectance as a function of aerosol absorption and surface reflectance

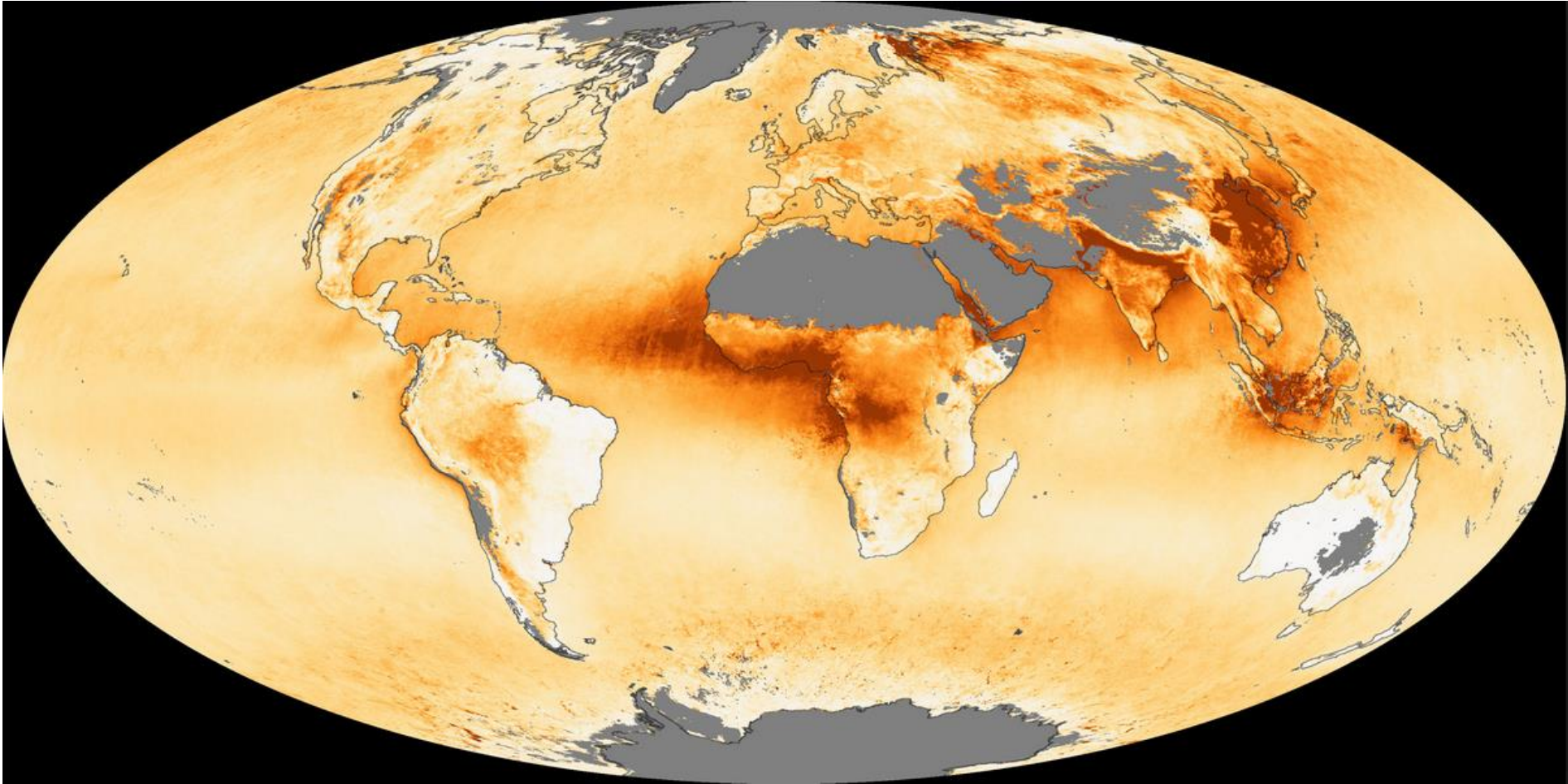


Figures in the two columns show changes in Top-of-Atmosphere Reflectance (Reflection Function), on y-axis, as a function of Aerosol Optical Thickness (or depth), on x-axis, as well as due to changes in surface reflectance (A_g).

The reflection function as a function of aerosol optical thickness and surface reflectance. The changing slope of each line depends on variations in surface reflectance.

MODIS Dark-Target AOD

In the Dark-Target retrieval algorithm, aerosols are retrieved over dark surfaces (vegetation, ocean), resulting in gaps over bright surfaces (deserts, above clouds and snow)



Surface Parameterization for Dark Target Algorithm

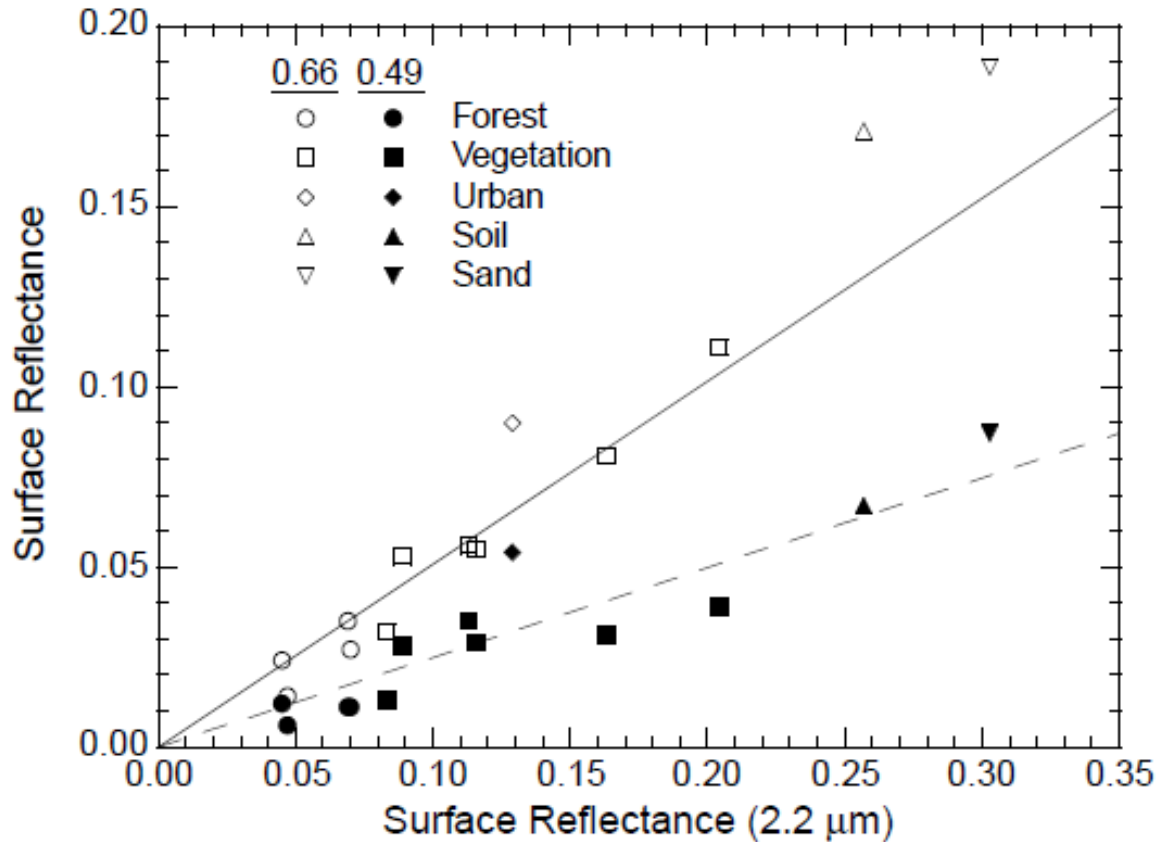
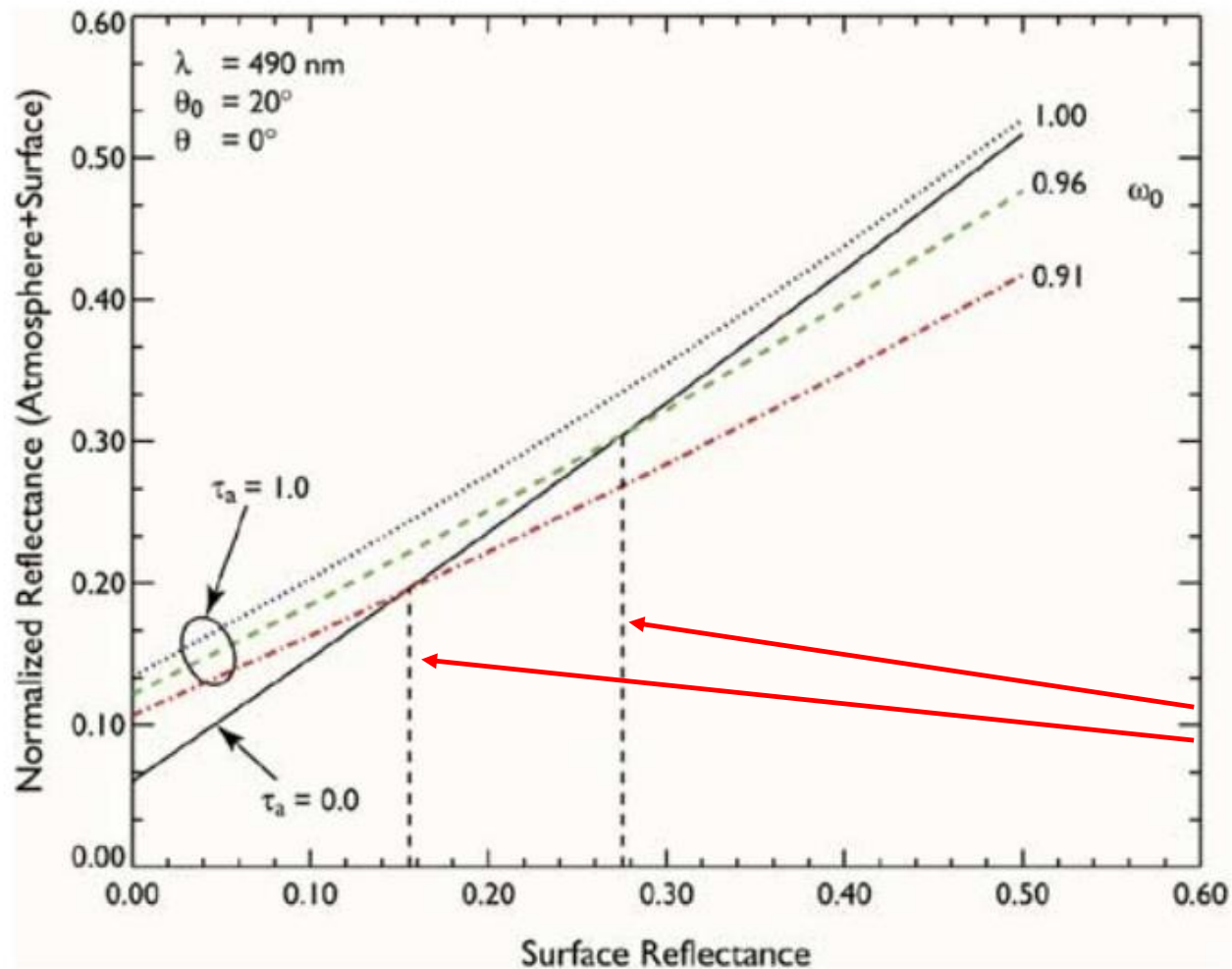


FIG. 3. Scatter diagram between the surface reflectance at 0.49 μm (solid symbols) and 0.66 μm (open symbols) to that at 2.2 μm , for several surface types. The average relationships $A_{0.49}/A_{2.2} = 0.25$ and $A_{0.66}/A_{2.2} = 0.5$ are also plotted (dashed and solid lines, respectively) (adapted from Kaufman et al. 1997b).

First, with the exception of dust, the aerosol optical thickness typically decreases with wavelength. Therefore aerosol optical thickness is 3–30 times smaller in the shortwave-infrared region than in the visible.

Second, surface reflectance across the solar spectrum is well correlated. Soils usually have a reflectance that increases as a function of wavelength, with a correlation that slowly decreases as the wavelength span increases.

Surface Reflectance at longer wavelengths (e.g. 2.2 micron, shown on x-axis) is used as a reference value, which is then linearly transformed to estimate the surface reflectance in the visible bands (e.g. 0.49 and 0.66 micron).



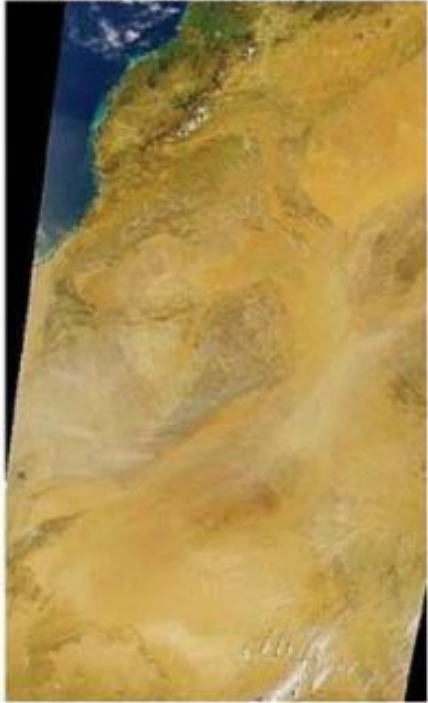
Critical Surface Reflectance

The vertical lines denote where detection of aerosols is difficult from satellite. This is because at higher surface reflectance values, it is difficult to distinguish between the underlying surface and overlying aerosol, from TOA.

Fig. 1. Simulated apparent reflectance (atmosphere + surface) at the top of the atmosphere at 490 nm, as a function of surface reflectance for various values of the aerosol optical thickness τ_a and single-scattering albedo ω_0 . The black solid line represents the apparent reflectance without aerosol, and the black dotted, green, and red lines represent the apparent reflectance with $\tau_a = 1.0$. The vertical lines denote the critical values of surface reflectance where the presence of aerosol cannot be detected by satellite for selected values of ω_n .

Hsu et al. 2004, TGRS

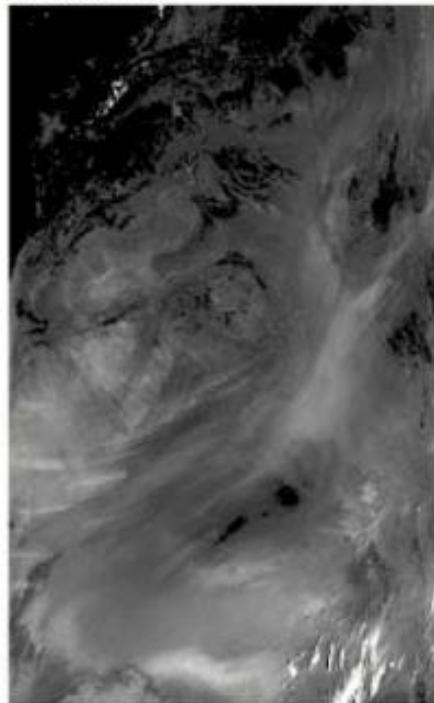
a) R(670, 555, 412 nm)



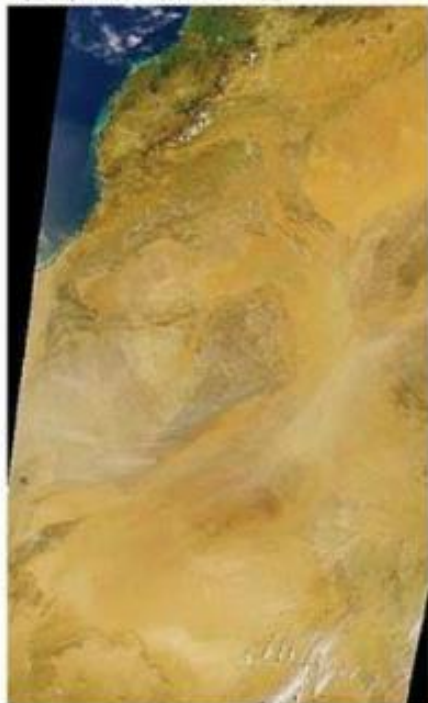
a) R(670, 555, 412 nm)



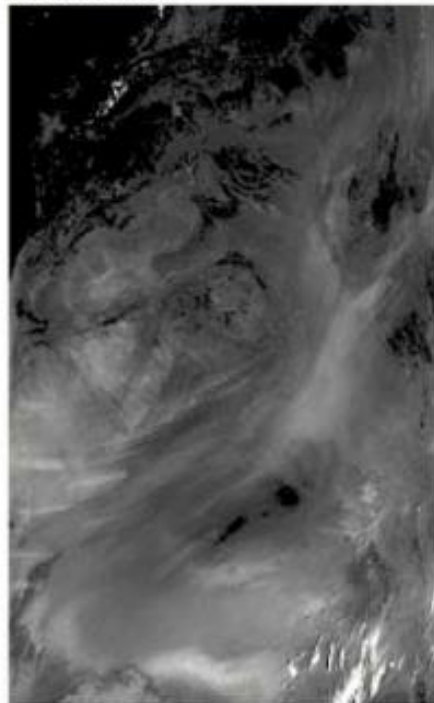
c) R(490 nm)



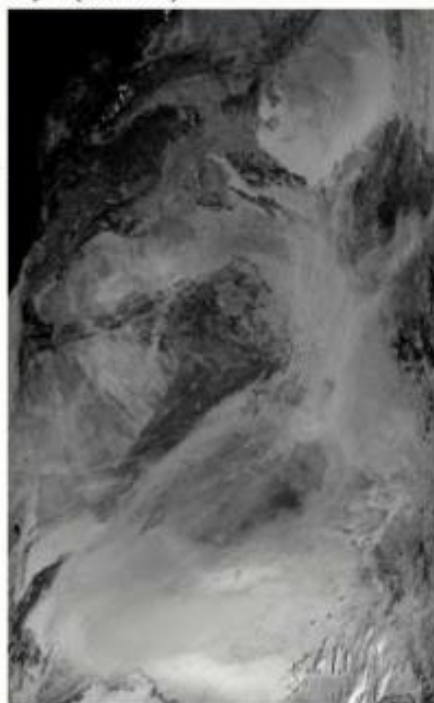
a) R(670, 555, 412 nm)



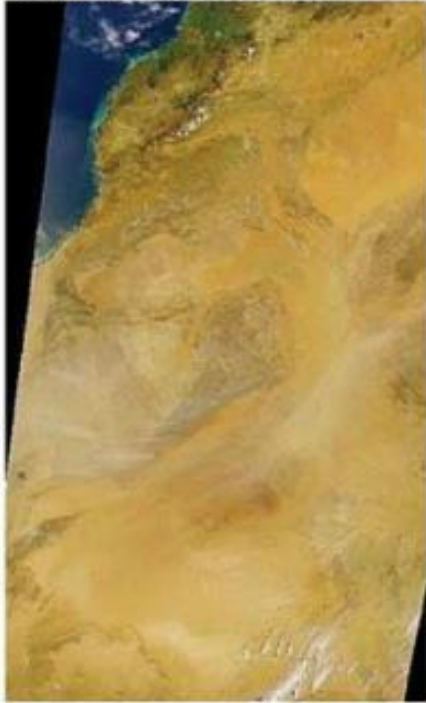
c) R(490 nm)



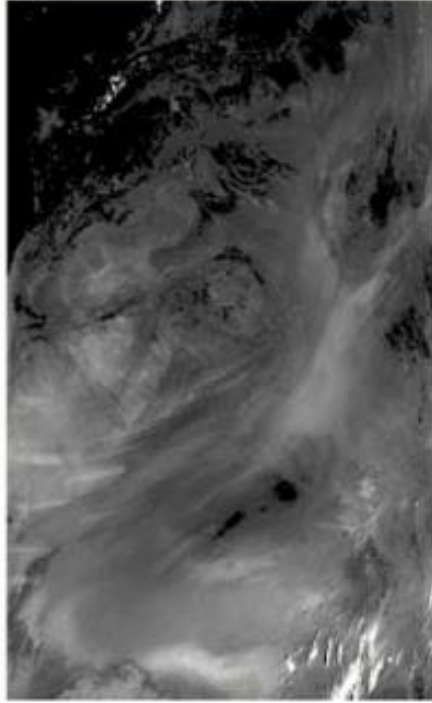
d) R(670 nm)



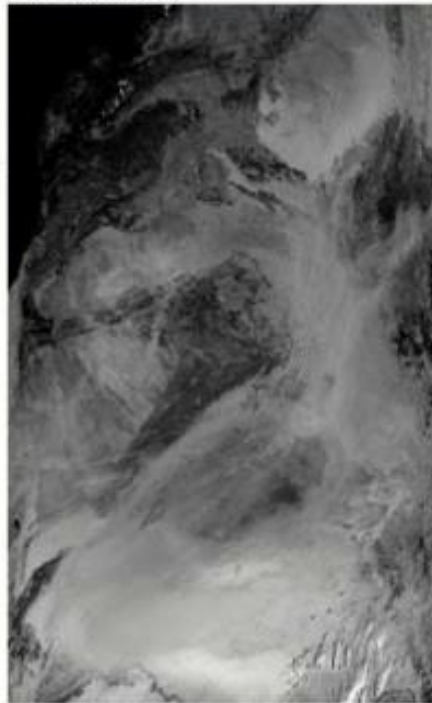
a) R(670, 555, 412 nm)



c) R(490 nm)



d) R(670 nm)



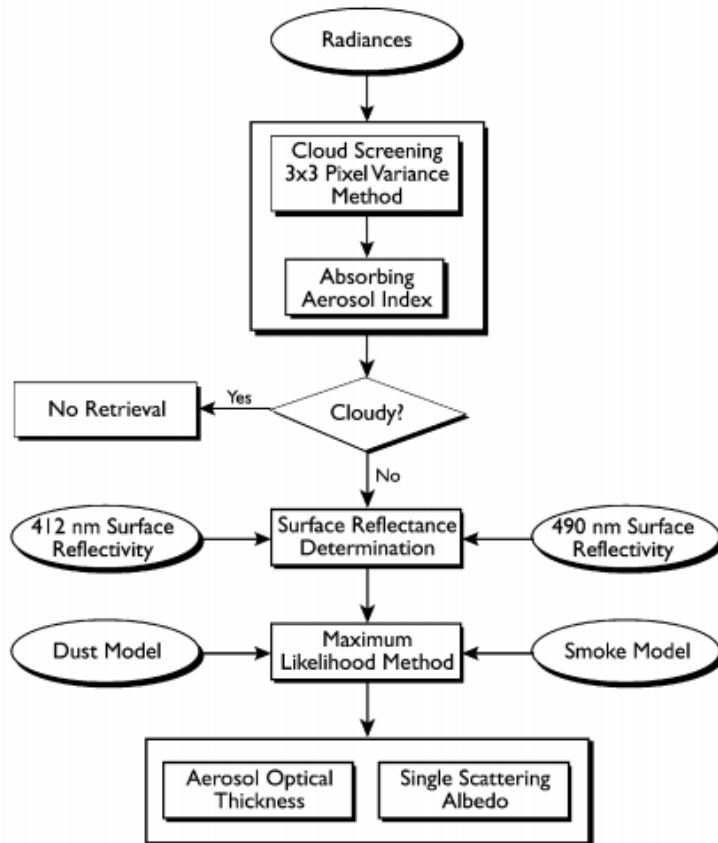
b) R(412 nm)



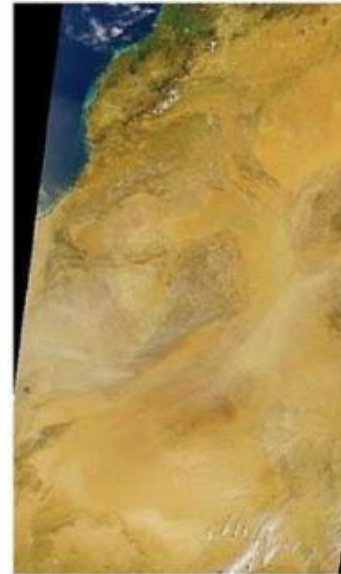
Hsu et al. 2004, TGRS

Basic Principle of MODIS Deep Blue Aerosol Algorithm over bright desert surfaces:

→ Instead of using reflectance at 490nm and 670nm, the deep blue algorithm uses the 412nm band where desert surface appears darker. As a result, it is easier to detect aerosols over desert at deep blue band (e.g. 412nm band).



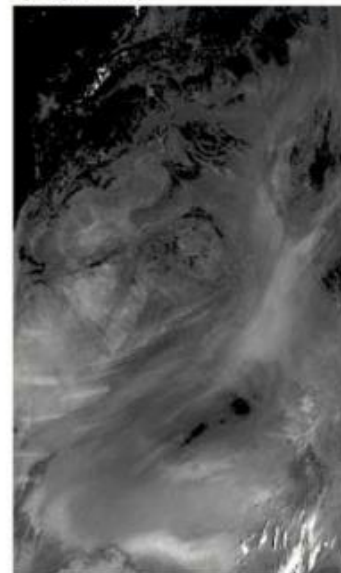
a) R(670, 555, 412 nm)



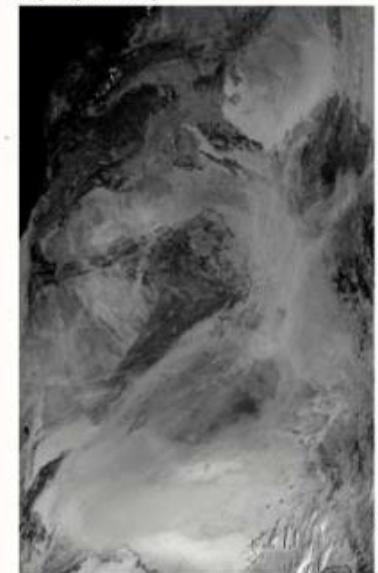
b) R(412 nm)



c) R(490 nm)

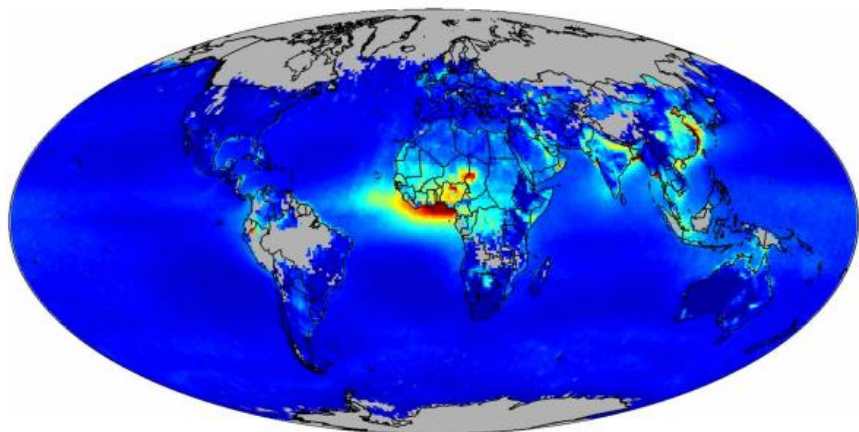


d) R(670 nm)

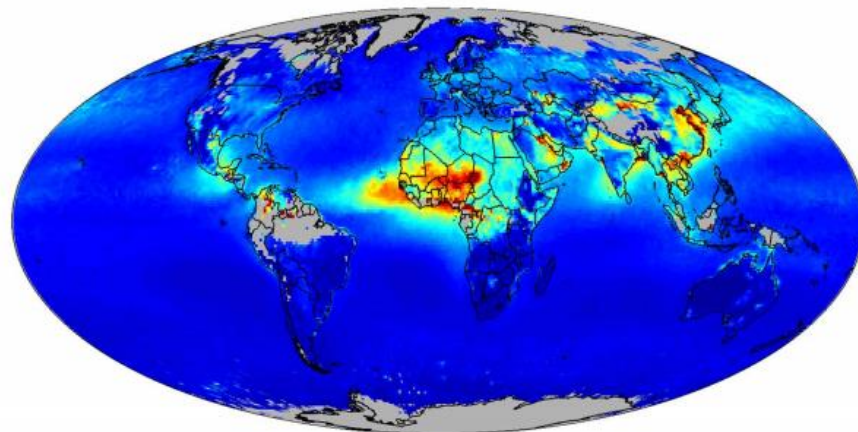


Deep Blue Aerosol Optical Depth

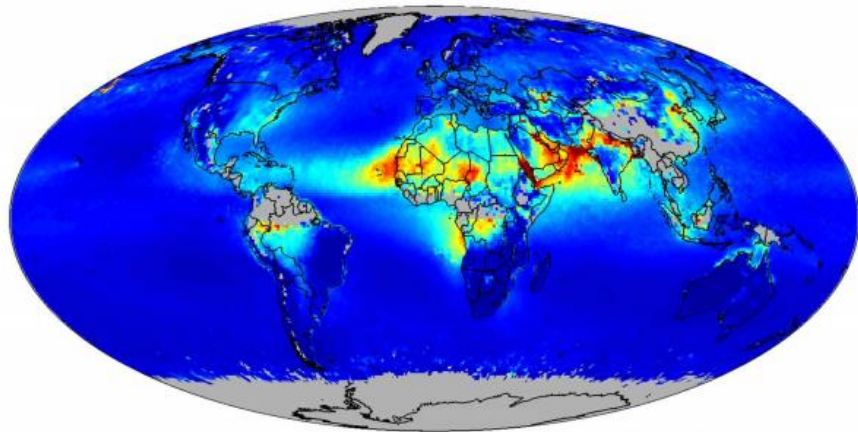
DJF



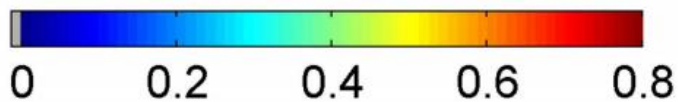
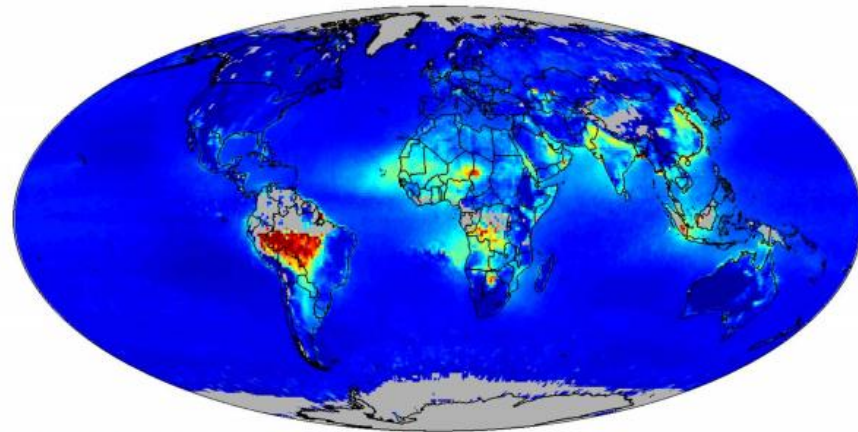
MAM



JJA

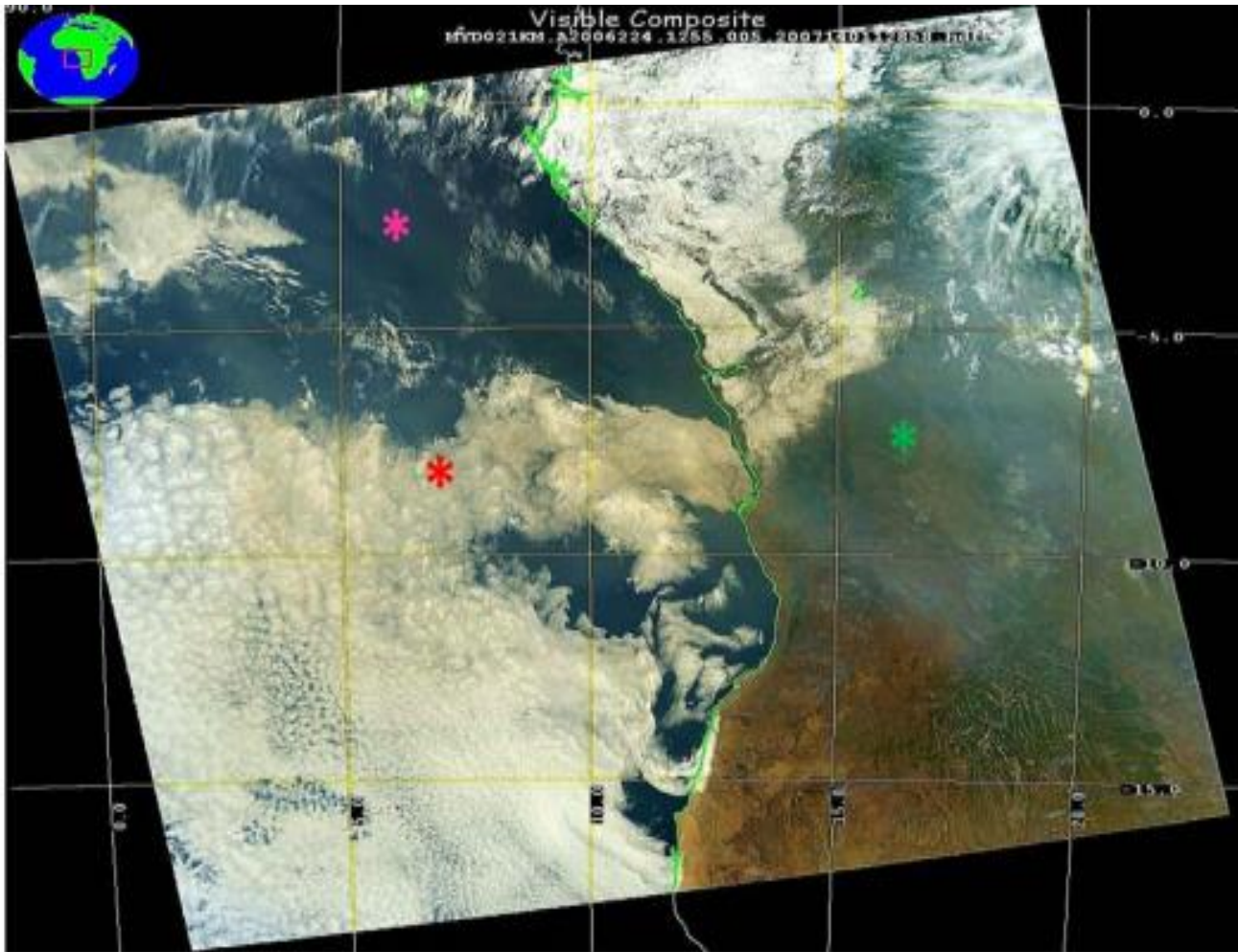


SON



Aerosol Remote Sensing over bright regions (e.g. Clouds)

In the case of aerosols above clouds, clouds appear darker due to multiple orders of reflections taking place between a bright surface such as the top of the cloud and the overlying aerosol layer. Refer to the red curves in the two plots below when smoke is above clouds and dust is above clouds.



Aerosol Remote Sensing over bright regions (e.g. Clouds)

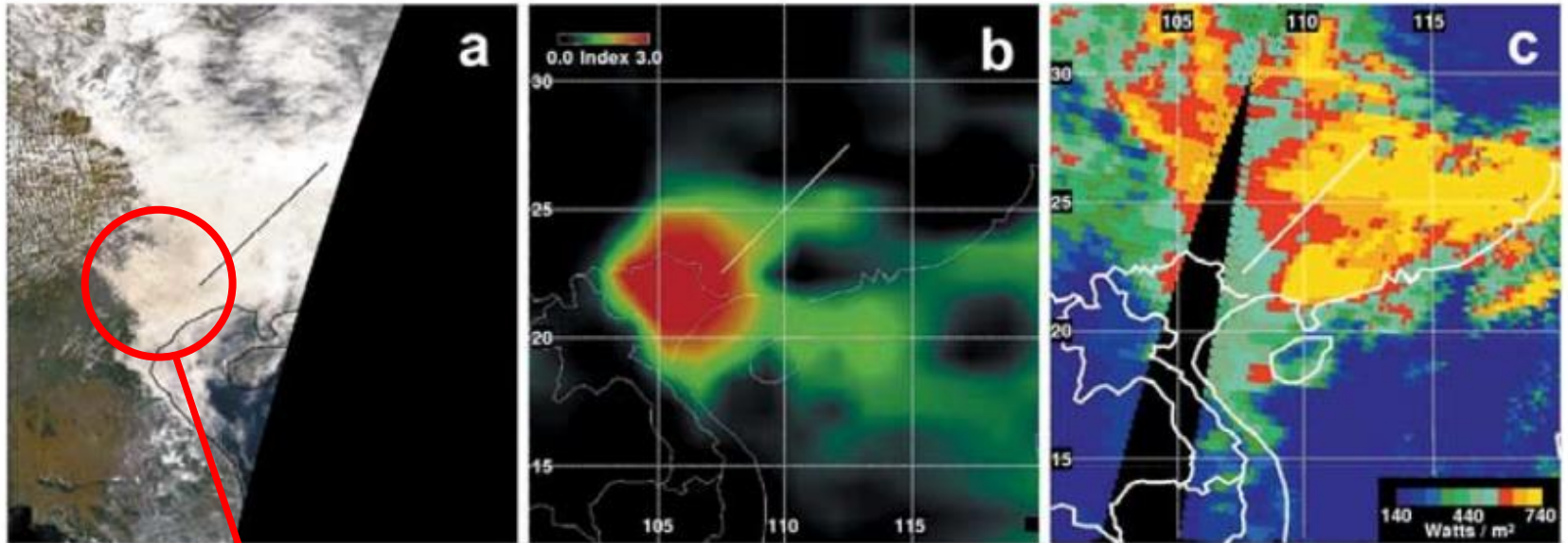


Figure 1. SeaWiFS true color image for Southeast Asia on 17 March 2000 is shown in (a), the corresponding TOMS AI in (b), and the CERES TOA upwelling shortwave flux in (c).

This area of the clouds appears to be darker than the rest of the cloudy region. It is also evident, in the figure on the right (panel c), that the upward reflected flux (in Wm^{-2}) is lower for the same region when aerosols are above cloud. The reflected flux values are significantly higher when there is not much aerosols above clouds ($>600 \text{ Wm}^{-2}$).

Aerosol Remote Sensing over bright regions (e.g. Clouds)

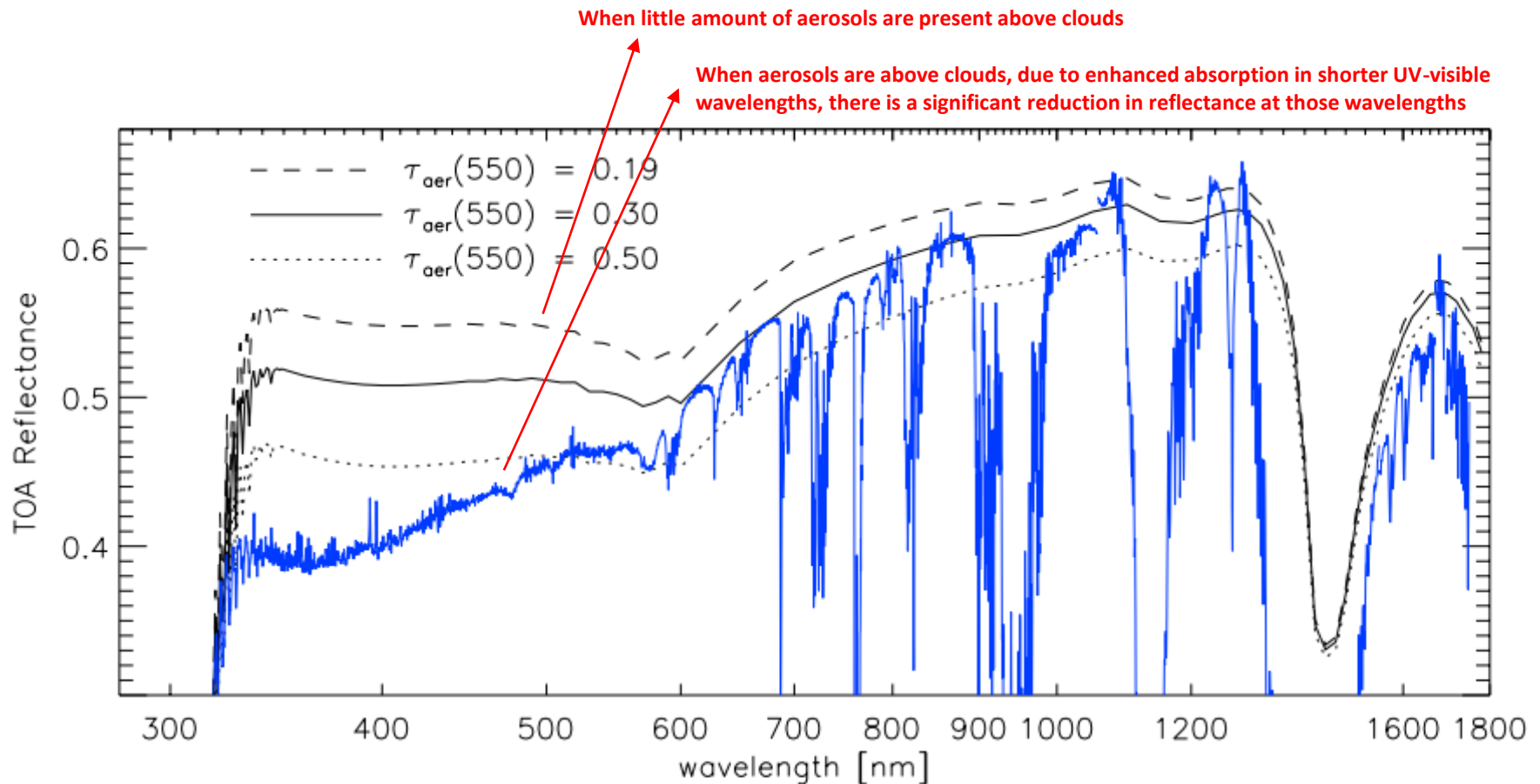


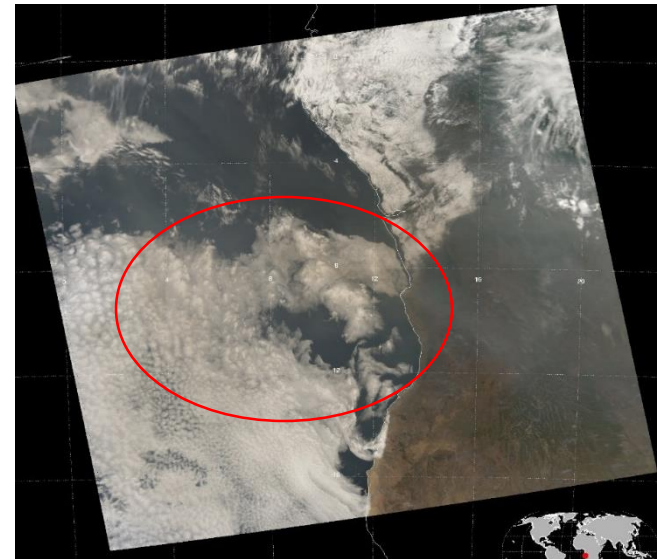
Figure 8. Multiple simulations of a smoke scene using model 3 (black lines), compared to the measured BBA scene (blue). The solid black line shows a fit to the measured reflectance spectrum, using a mixture of 99.5% aerosols in number density, corresponding to an aerosol optical thickness at 550 nm of 0.30, which is the same as the AOT of model 1. The reflectance spectra of layers with an AOT of 0.19 and 0.50 are shown for comparison by the dashed and the dotted line, respectively.

Satellite Snapshots of Smoke above Clouds

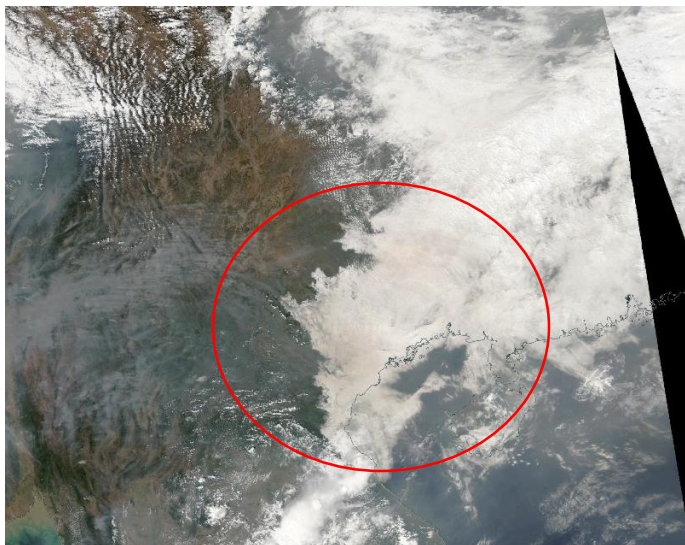
Northern Canada



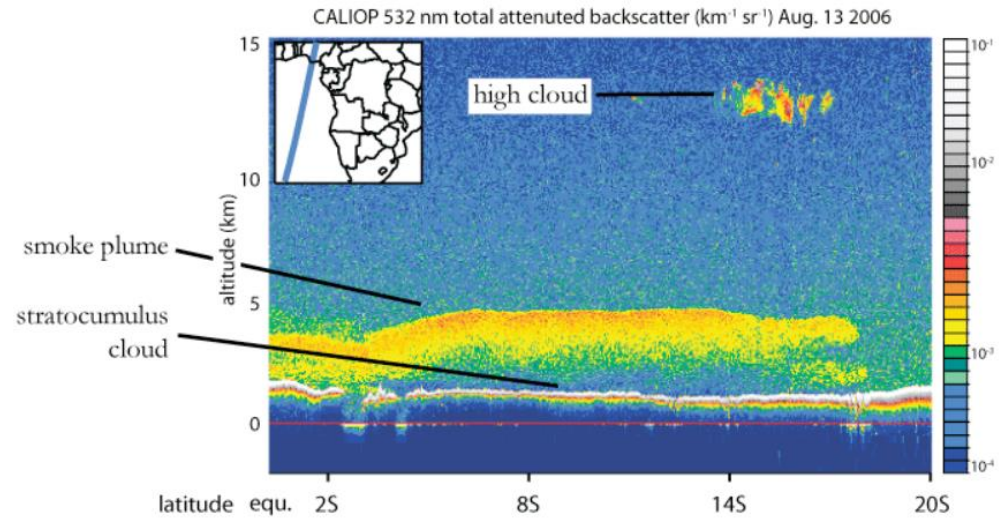
Southeast Atlantic



Southeast Asia



Southeast Atlantic (CALIOP data, Wilcox et al. 2010)



Another case of Clouds embedded in Smoke from CAR, resulting in observed darkening

